NAVAL
POSTGRADUATE
SCHOOL

MONTEREY, CALIFORNIA

THESIS

FREE ELECTRON LASER STABILITY EFFECTS AND DESIGN OF AN ELECTROSTATIC CATHODE TEST CELL

by

Robert L. Edmonson III

December 2009

Thesis Co-Advisors:　　　　William B. Colson
　　　　　　　　　　　　　Joseph Blau

Approved for public release; distribution is unlimited

REPORT DOCUMENTATION PAGE		*Form Approved OMB No. 0704-0188*
Public reporting burden for this collection of information is estimated to average 1 hour per response, including the time for reviewing instruction, searching existing data sources, gathering and maintaining the data needed, and completing and reviewing the collection of information. Send comments regarding this burden estimate or any other aspect of this collection of information, including suggestions for reducing this burden, to Washington headquarters Services, Directorate for Information Operations and Reports, 1215 Jefferson Davis Highway, Suite 1204, Arlington, VA 22202-4302, and to the Office of Management and Budget, Paperwork Reduction Project (0704-0188) Washington DC 20503.		
1. AGENCY USE ONLY *(Leave blank)*	**2. REPORT DATE** December 2009	**3. REPORT TYPE AND DATES COVERED** Master's Thesis
4. TITLE AND SUBTITLE Free Electron Laser Stability Effects and Design of an Electrostatic Cathode Test Cell		**5. FUNDING NUMBERS**
6. AUTHOR(S) Edmonson III, Robert L.		
7. PERFORMING ORGANIZATION NAME(S) AND ADDRESS(ES) Naval Postgraduate School Monterey, CA 93943-5000		**8. PERFORMING ORGANIZATION REPORT NUMBER**
9. SPONSORING /MONITORING AGENCY NAME(S) AND ADDRESS(ES) N/A		**10. SPONSORING/MONITORING AGENCY REPORT NUMBER**
11. SUPPLEMENTARY NOTES The views expressed in this thesis are those of the author and do not reflect the official policy or position of the Department of Defense or the U.S. Government.		
12a. DISTRIBUTION / AVAILABILITY STATEMENT Approved for public release; distribution is unlimited		**12b. DISTRIBUTION CODE** A
13. ABSTRACT (maximum 200 words) Developing the Free Electron Laser (FEL) as a weapon is of high interest to the United States Navy. This thesis aims to gain insight, through simulation of generic configurations of an oscillator and amplifier FEL, into the performance of an FEL and the effects of electron beam misalignments. It then compares simulation results to an existing experiment, and explores similarities and differences. 　　Additionally, a new cathode test cell is designed. Electrostatic cathode test cell designs are proposed and a recommendation for future design and construction is made.		
14. SUBJECT TERMS Free Electron Laser, FEL, Misalignment, Mirror, Electron Beam, Optical Field, Cathode, Test Cell, Electron Gun		**15. NUMBER OF PAGES** 105
		16. PRICE CODE
17. SECURITY CLASSIFICATION OF REPORT Unclassified	**18. SECURITY CLASSIFICATION OF THIS PAGE** Unclassified	**19. SECURITY CLASSIFICATION OF ABSTRACT** Unclassified **20. LIMITATION OF ABSTRACT** UU

i

THIS PAGE INTENTIONALLY LEFT BLANK

FREE ELECTRON LASER STABILITY EFFECTS AND DESIGN OF AN ELECTROSTATIC CATHODE TEST CELL

Robert L. Edmonson III
Lieutenant, United States Navy
B.S., Oregon State University, 2003

Submitted in partial fulfillment of the
requirements for the degree of

MASTER OF SCIENCE IN APPLIED PHYSICS

from the

**NAVAL POSTGRADUATE SCHOOL
December 2009**

Author: Robert L. Edmonson III

Approved by: William B. Colson
                 Thesis Advisor

                 Joseph Blau
                 Co-Advisor

                 Andres Larraza
                 Chairman, Department of Physics

iii

THIS PAGE INTENTIONALLY LEFT BLANK

ABSTRACT

Developing the Free Electron Laser (FEL) as a weapon is of high interest to the United States Navy. This thesis aims to gain insight, through simulation of generic configurations of an oscillator and amplifier FEL, into the performance of an FEL and the effects of electron beam misalignments. It then compares simulation results to an existing experiment, and explores similarities and differences.

Additionally, a new cathode test cell is designed. Electrostatic cathode test cell designs are proposed and a recommendation for future design and construction is made.

THIS PAGE INTENTIONALLY LEFT BLANK

TABLE OF CONTENTS

THIS PAGE INTENTIONALLY LEFT BLANK

LIST OF FIGURES

THIS PAGE INTENTIONALLY LEFT BLANK

LIST OF TABLES

THIS PAGE INTENTIONALLY LEFT BLANK

ACKNOWLEDGMENTS

To my loving wife, Melissa, thank you. The love, patience and encouragement that you give me are truly amazing. I cherish you and our family and look forward to a lifetime of chasing dreams together.

THIS PAGE INTENTIONALLY LEFT BLANK

I. INTRODUCTION

Using the Free Electron Laser (FEL) as a weapon system has been in the research phase for several decades. Recently, however, the United States Navy has become more committed to a weapon design phase, as indicated by a letter to the Strategic Studies Board [1] ordering the study into the viability of using directed energy weapons. Also, Office of Naval Research (ONR) is beginning the FEL Innovative Navy Prototype (INP), starting in 2010. These steps have given direction and committed resources to the development of the FEL as a viable weapon system. This highlights the importance of further research and understanding into the physics of the FEL operation and limitations. This thesis uses simulations to evaluate this FEL performance and introduces a design for an electrostatic cathode test cell for use at the Naval Postgraduate School (NPS). This test cell will be used for further research opportunities into the cathode operation and selection in future FEL configurations.

Chapter II reviews the major components of the FEL system. First, it explores the generation of the electron beam in the injector and its subsequent increase in energy through the superconducting accelerator. Once relativistic, the electron beam enters the undulator in order to generate coherent light. The FEL is presented in two layouts: (1) In the oscillator design, the light passes many times between the two mirrors, allowing for energy exchange and growth of the optical field, and (2) the amplifier layout, using a longer undulator that creates a

high power from a seed laser in one pass through the undulator. Finally, the principle of recirculation of the electron beam is introduced, allowing for a more efficient machine, and the means by which the electrons are disposed of at lower energy.

Chapter III reviews the FEL characteristics. A key feature of the FEL is that it can be designed to operate over a wide range of wavelengths in the electromagnetic spectrum and can be tuned for a given design to optimize the operating wavelength.

Chapter IV reviews the basic theory of the FEL, emphasizing how the FEL is able to generate and then amplify light. The electron photon race demonstrates that at resonance the optimum energy exchange between electron and the optical field occurs. The pendulum and wave equation derivation then describes how energy is exchanged between the electrons and the optical field.

New research is then presented in Chapter V through Chapter VII. First, a generic oscillator is simulated with various misalignments in the electron beam. Its performance is analyzed and then compared to a generic amplifier in Chapter VI. Both are similar in parameters in order to compare the sensitivity to similar misalignments in two different undulator configurations. Chapter V also uses the same comparison philosophy on an existing experiment, notes the differences, and explores possible sources of this difference.

In Chapter VII, a design is proposed for the first electrostatic cathode test cell at NPS. When built, the test cell will allow NPS to explore a new area of research.

This design would open the door for collaboration on potential cathode designs that will eventually be used in the Navy's FEL weapon. Additional analysis is presented explaining field emission from a cold metal and space charge limited current in the proposed cathode. Multiple geometries are explored using an electrostatic field modeling code and then a final recommendation is made for future students.

THIS PAGE INTENTIONALLY LEFT BLANK

II. FEL COMPONENTS

Two configurations of the free-electron laser (FEL) are the oscillator and amplifier. Many components are common to both designs, as seen in Figure 1. In an oscillator configuration, radiation energy is stored in the optical cavity. In the amplifier configuration there is no optical cavity and the amplification of light must occur in one pass. A seed laser beam introduced at the beginning of the undulator is amplified in a single pass, as shown in Figure 1. The following discusses the purpose and general properties of the FEL system components. The discussion depicts the energy recovery linear accelerator (ERL) with a superconducting accelerator, but it should be mentioned that not all FELs are ERLs or include the super-conducting accelerators.
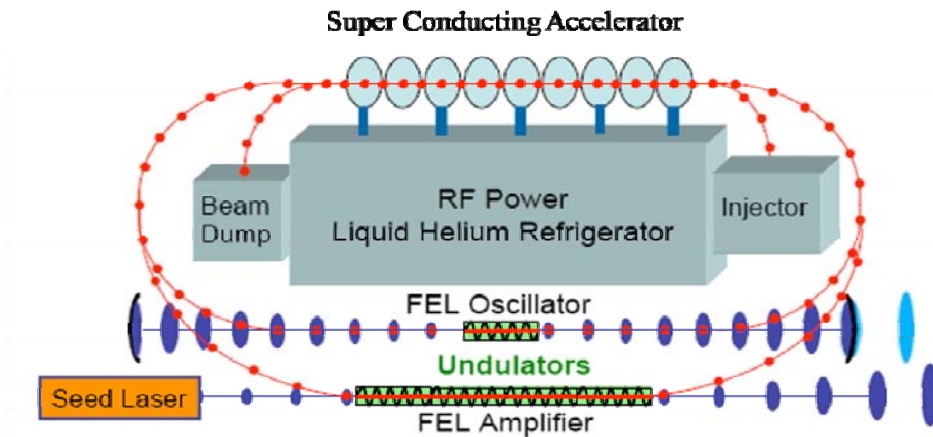
Figure 1.   This schematic depicts the core components of an FEL. Two options shown, run as an amplifier or an oscillator. In blue are the optical pulses and in red are the electrons. This system includes a) separate beam paths for running as an oscillator or amplifier; b) a superconducting accelerator and its associated refrigeration plant; and c) energy recovery (beam recirculation). [From 2].

A.   INJECTOR

The first step in the process is the liberation of an electron bunch from a cathode. Two examples of how this is accomplished are thermionic emission and photoemission. In thermionic emission, the cathode is heated in order to "boil" off electrons. Photoemission, on the other hand, occurs when photons from a drive laser strike the surface of the cathode to release electrons from its surface. Because we want a well-collimated beam with a small energy spread, beam quality is a major concern, it is important that the cathode design and the method of ejection of electrons be precise. Poor quality will propagate irretrievably through the laser system and will degrade the laser interaction. To achieve high quality, a high voltage in the injector accelerates the electrons away from the cathode up to relativistic speeds before the effects of space charge cause the beam to spread.

B.   ACCELERATOR

Once the electrons, with energy of approximately 5-10 MeV, have arrived at the accelerator in bunches, it is necessary to increase their energy by roughly one order of magnitude. An efficient method to do this is with a superconducting radio frequency (SRF) accelerator, as shown in Figure 2.
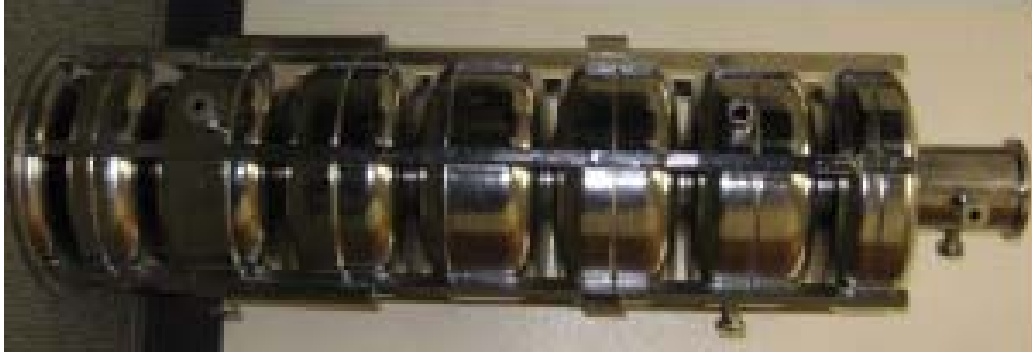
Figure 2.   Superconducting accelerator cavity used to increase the energy of the electrons from the injector to levels needed for the FEL interaction in the undulator. The cavities are ellipsoidal in shape, and there are ports to inject the radio frequency fields. The electron travels through the center of the cavity space.

A klystron supplies RF energy at the frequency of the electron pulses and generates alternating fields in a series of cavities that the electrons pass through. By design, the electron pulses enter the cavity in phase with the field, take energy from the field, and are accelerated to approximately 100 MeV. Since the electrons are traveling in pulses, the leading edge may reach a given cavity off the optimum phase so that it will accelerate to a different value from the center of the pulse. Conversely, the trailing edge, where the electrons are traveling slightly slower, may be given an extra boost in energy. The result of this is further compacting of the pulse.

C. UNDULATOR
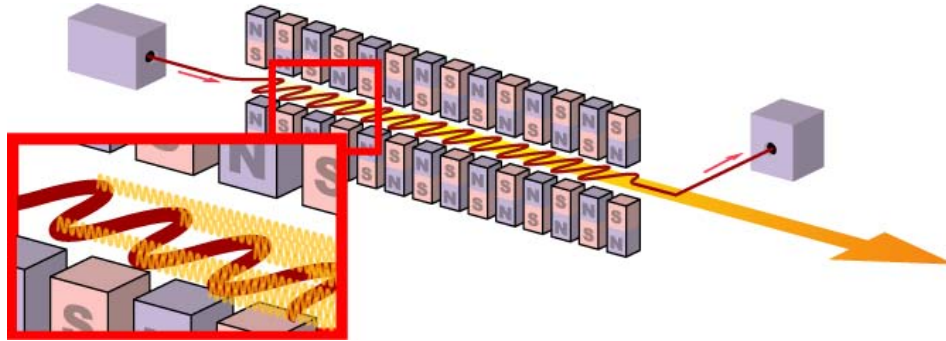
Figure 3.   Undulator, a schematic representation. In red is the electron beam undergoing transverse oscillations. The undulator magnets have alternating north and south poles. The stimulated emission in yellow propagates on axis in a forward direction in reference to the electron motion. [From 3].

The relativistic beam of bunched electrons then travels through the undulator, as seen in Figure 3. The pulse of electrons travel through the periodic magnetic fields of alternating dipole magnets. In the presence of these periodic fields, the electrons accelerate by the Lorentz force in the transverse direction in a sinusoidal "wiggling" path. As the electrons "wiggle," they emit photons; the strength and spacing of the magnets and the energy of the electrons determining the wavelength. The relativistic speed of the electrons ensures that light is emitted in a narrow forward beam propagating along the axis of the optical cavity. In a free electron oscillator, the light pulse is reflected back through the cavity to meet the next incoming bunch. Stimulated emission is the mechanism by which a small fraction (~few percent) of the energy of the electron beam transfers to the optical beam.

D.   OSCILLATOR DESIGN

The first design we consider for weapons application is the oscillator, shown in Figure 4. The undulator is contained in the resonator cavity, with a fully reflective mirror at one end and a partially transmissive mirror at the other. The initial source of light for the optical field is spontaneous emission. Over many reflected passes of light, interaction with the radiating electron beam results in amplification (stimulated emission) of coherent light. Because energy must be stored in the optical cavity, a near-concentric (short Raleigh length) cavity may be used. The curvature and spacing of the mirrors determines the Raleigh length, which causes the radius of the optical mode to vary from roughly 3 cm at the mirrors to 0.1 mm at the center of the undulator. This allows for good interaction between the electron beam and optical mode through the undulator and keeps the intensity at the mirrors to a relatively low level without having to separate them by unreasonably large distances. The spacing of the mirrors is such that as each pulse of light reflects between mirrors as it enters the undulator in proper phase with the electron pulse.
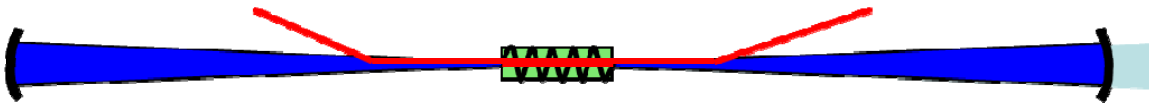
Figure 4.   Generic Oscillator schematic. The interaction of the electron pulses (red) with the optical field (blue). The electron beam pulses enter the (green) undulator in phase with the optical laser pulses; transfer energy to the optical pulse, then exits the optical cavity. The partially transmitting mirror on the right allows a fraction of the stored energy to exit the cavity.

9

E.   AMPLIFIER DESIGN

The basic layout of the amplifier design is shown in Figure 5.   The source of initial optical pulse in an amplifier design is a seed laser, rather than spontaneous emission in an oscillator.   The seed laser emits pulses of light along the optic axis in sync with the incoming electrons.   The light only gets one pass to reach a large saturated power, as opposed to many passes in the case of the oscillator.   The short Raleigh length proposed for the oscillator does not apply.   As a result, the light pulse must travel much further before it strikes the first optical element in order for the intensity to decrease to levels that will not damage the mirror.

In order to improve extraction in a long wiggler, it is necessary to include a taper in the magnetic field strength.   The taper allows extraction to continue after a point at which saturation would occur without the taper. Increasing the transverse gap between the magnets, thereby slightly reducing their on-axis field is a typical method for accomplishing the taper.
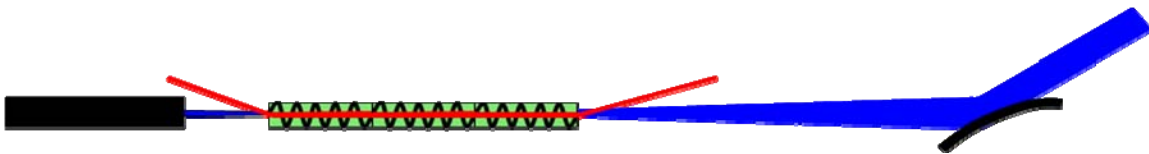
Figure 5.   Generic amplifier schematic. In red is the electron beam that has been steered into the undulator. In green is the undulator where the interaction between the electron beam and the optical field takes place. The undulator magnetic field is in black and in blue is the optical field. The seed laser on the left also in black. The mirror on the right is representative of the first step of the beam transport path.

10

F.   BEAM RECIRCULATION AND DISPOSAL

Extracting energy from the electron beam for optical field growth will only decrease its energy by a few percent. This leaves a very high-energy electron beam that must be disposed of. In many applications, it is common to proceed straight to a beam dump, which consists of an absorbing metal target that will dissipate the energy in the form of heat. This heat is then removed by external cooling such as water. For shipboard applications, however, the Bremsstrahlung radiation created by these high energies would provide hazard that would require great amounts of shielding, conflicting with space constraints and adding unwanted weight. To solve this problem, magnets direct the beam to pass through the accelerator again but this time out of phase with the RF field that accelerated it originally. The beam thereby gives up a substantial amount of its energy to the accelerator fields and enters the beam dump downstream from the accelerator, with energy of approximately 5-10 MeV. At this energy, no neutrons are produced, significantly reducing shielding requirements, and much less RF power will be needed to maintain the accelerator fields for subsequent electron pulses from the injector. Thus, overall efficiency vastly improves. This is referred to as an energy recovery linear accelerator (ERL).

THIS PAGE INTENTIONALLY LEFT BLANK

III. FEL CHARACTERISTICS

A. TUNABILITY VS DESIGNABILITY

In a conventional laser, the properties of the light generating medium determine the wavelength produced. The FEL is the first laser that can be designed to operate at almost any wavelength in the electromagnetic spectrum, and is tunable over a large range. By changing the strength of the magnetic field of the undulator, or the spacing of the magnets, or the energy of the electron beam, the FEL can achieve wavelength ranges not possible with conventional lasers. This is important for military applications in order to design to a wavelength that will propagate well through the atmosphere. It could also be useful for designing an FEL amplifier that will operate at a wavelength where there are high power, commercially available (or relatively easy to build) seed lasers.

B. POWER LEVEL AND RELIABILITY

Since there is no solid-state or gas medium, inside of which the light is being generated, in an FEL, heating of the laser medium is not an issue at high powers. Mirror heating may be a problem as with any high power laser. In addition, existing FELs are very reliable. They run in laboratories such as Stanford and Jefferson Lab twenty-four hours a day, seven days a week. High power ERL-based FELs could have wall-plug efficiencies up to 20%. The final advantage of the FEL is that it uses electricity instead of dangerous chemicals or gasses to generate light. This allows for less restrictive and cumbersome use of the weapon, which is therefore much safer for personnel. In

addition, there is no "magazine limit," as long as ship fuel is available; a single engagement with an FEL weapon should only use a few gallons of ship fuel.

IV. BASIC THEORY

A laser is a coherent light source. In a conventional laser, the electrons that are used to create this light are in a gaseous or solid-state material. They are placed in an energized state that will enable them to emit light, a process referred to as "pumping." Since there is an absorbing material, the energy put into the system and given off generates a lot of heat that needs to be dissipated. In a free electron laser, the electrons eject or "boil off" the injector as described in the previous chapter and are no longer in a bound state. While in the undulator, they are accelerated using magnetic fields, governed by the Lorentz Force equations. This acceleration causes the emission of light without heating up the cavity. When there is light present then the electromagnetic field also affects the motion of the electrons and energy can be exchange between the electrons and the field. In this section, we look at the basic principles governing the Free Electron Laser to understand how it is able to generate and amplify light.

A. RESONANCE CONDITION

Resonance occurs when energy transfer between the electrons and the optical field is optimum. To elaborate, electrons travel down the undulator axis at a speed $\beta_z c$, while the optical pulse is traveling at the speed of light, c. The relationship between the two speeds results in the "electron-photon race," depicted in Figure 6.
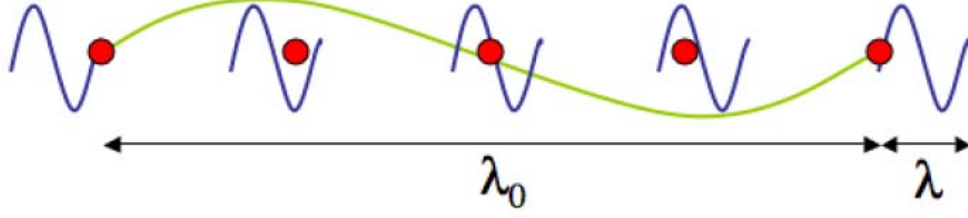
Figure 6.   Electron-Photon Race. The blue represents an optical wavelength; the green is the undulator wavelength and the red dot the electron's position within an optical wavelength at different locations along the undulator. The electron has lost the race by one wavelength of light in a single undulator period.

Using the difference in speeds between the two race participants where the light is leading the electron by velocity

$$c(1 - \beta_z) \ , \tag{1}$$

one can calculate the winning distance, λ. By multiplying the velocity difference by the time that the race,

$$\Delta t = \lambda_0 \big/ \beta_z c \ , \tag{2}$$

we see that the laser wavelength at the resonance condition is

$$\lambda = c(1 - \beta_z)\Delta t \ ,$$
$$\lambda = \lambda_o \frac{1 - \beta_z}{\beta_z} \ . \tag{3}$$

The relativistic Lorentz force equations that govern an electron's motion are

$$\frac{d(\gamma \vec{\beta})}{dt} = -\frac{e}{mc}\left(\vec{E} + \vec{\beta} \times \vec{B}\right) \ , \tag{4}$$

$$\frac{d\gamma}{dt} = -\frac{e}{mc}\vec{\beta} \cdot \vec{E} \ , \tag{5}$$

16

where $c\vec{\beta} = \vec{v}$ is the electron velocity, m is the electron mass, and e is the electron charge. The relativistic Lorentz factor, γ, gives the relationship between the electron's velocity and its energy

$$\gamma^{-2} = 1 - \beta_\perp^2 - \beta_z^2 \ . \tag{6}$$

The undulator parameter, which is a dimensionless measure of the undulator field strength B_{rms}, is

$$K = \frac{eB_{rms}\lambda_o}{2\pi mc^2} \ . \tag{7}$$

For a relativistic electron beam, $\gamma \gg 1$, we can show that [2]

$$\beta_z \approx \frac{1 - \left(1 + K^2\right)}{2\gamma^2} \ . \tag{8}$$

We can now rewrite the condition for resonance in terms of K

$$\lambda \approx \frac{\lambda_0(1 + K^2)}{2\gamma^2} \ . \tag{9}$$

B. PENDULUM EQUATION

For a helical undulator the magnetic field along the axis is

$$\vec{B} = B_m[\cos(k_o z), \sin(k_o z), 0] \ . \tag{10}$$

In this equation $B_m = B_{rms}$ is the magnetic field strength, $\lambda_o = 2\pi/k_o$ is the undulator period and z is the distance along the undulator. The optical electric and magnetic fields are

$$\vec{E} = E[\cos(\psi), -\sin(\psi), 0] \ , \tag{11}$$

$$\vec{B} = E[\sin(\psi), \cos(\psi), 0] \ . \tag{12}$$

17

In these equations $\psi = kz - \omega t + \phi$, E is the optical field amplitude in cgs units, ϕ is the optical phase, $k = 2\pi/\lambda$ is the wavenumber and $\omega = kc$ is the frequency.

Substituting the undulator and laser fields into the Lorentz force equation, (4) and realizing that for relativistic electrons the speed is almost the speed of light, c, the transverse motion of an electron in a helical undulator is [2]

$$\vec{\beta}_\perp = \left(-\frac{K}{\gamma}\right)\left[\cos(k_o z), \sin(k_o z), 0\right] \quad . \tag{13}$$

We then look at the electron's microscopic motion. By substituting equation (11) and (12) into (3) we find

$$\dot{\gamma} = \frac{eKE}{\gamma mc}\cos(\zeta + \phi) , \tag{14}$$

where $\zeta = (k + k_o)z - \omega t$ is the "electron phase." The electron phase follows the electron's microscopic position $z(t)$ within an optical wave. Also, note that if $\dot{\gamma} > 0$, the electron gains energy, if $\dot{\gamma} < 0$, the electron loses energy to the optical field. For a random distribution of the electron phases, about half the electrons gain energy and half lose energy. This causes the electron beam to bunch and to radiate coherently.

We introduce the electron phase velocity as

$$\nu \equiv \frac{d\zeta}{d\tau} = L[(k + k_0)\beta_z - k], \tag{15}$$

where we have taken the derivative of the electron phase with respect to dimensionless time, $\tau = ct/L$. Using this scale for time, we see that τ goes from 0 to 1 along the length of the undulator, L. Next, we take the derivative

of the electron phase velocity and use the previous result that at resonance $\beta_z \approx 1-(1+K^2)/2\gamma^2$ in the relativistic limit of $\gamma \gg 1$ to get

$$\frac{d\nu}{d\tau} = \overset{\circ}{\nu} = \frac{4\pi L}{\lambda_\circ} \frac{d\overset{\circ}{\gamma}}{\gamma} \quad . \tag{16}$$

We can arrive at the "pendulum equation" by combining equation (14) and equation(16) to get

$$\overset{\circ}{\nu} = \overset{\circ\circ}{\zeta} = |a| \cos(\zeta + \phi) \ , \tag{17}$$

where $|a|=4\pi NeKLE/(\gamma^2 mc^2)$ is the dimensionless laser field amplitude and expresses how more relativistic electrons with larger Lorentz factor, γ, require a stronger optical field E or a longer undulator to accomplish the same bunching. When $|a| \leq \pi$, the laser has weak optical fields, the electrons do not strongly bunch, and there is insignificant energy exchange between the electrons and the optical fields. When $|a| \gg \pi$, the laser has strong fields and there can be significant bunching and energy exchange. The pendulum equation (17) describes the microscopic motion of electrons in phase space and is valid in both weak and strong optical fields with high or low gain.

C. WAVE EQUATION

Maxwell's wave equation written in the full form is

$$\left(\frac{\partial^2}{\partial x^2} + \frac{\partial^2}{\partial y^2} - \frac{1}{c^2}\frac{\partial^2}{\partial t^2}\right)\vec{A}(\vec{x}, t) = -\frac{4\pi}{c}\vec{J}_\perp(\vec{x}, t) \ , \tag{18}$$

where the optical vector potential is $\vec{A}(\vec{x},t)$, c is the speed of light, and $\vec{J}_\perp$ is the transverse component the electron

current density. Using the following relationships, we are
able to derive the laser's electric and magnetic fields

$$\vec{E} = -\frac{1}{c}\frac{\partial \vec{A}}{\partial t} \quad , \tag{19}$$

$$\vec{B} = \vec{\nabla} \times \vec{A} \quad . \tag{20}$$

We assume that the beam is coherent, that the optical
vector potential is slowly varying over the optical
wavelength, and that it is slowly varying in time compared
to the optical frequency. Next, put the vector potential
in the form

$$\vec{A} = \frac{E(\vec{x}, t)}{k}\hat{\varepsilon}e^{i\alpha} \quad , \tag{21}$$

where $\alpha=kz-\omega t$ is the phase of the carrier wave, E is the
complex laser electric field and $\hat{\varepsilon}$ is the laser field's
polarization vector. Using the "method of characteristics"
we can derive that the parabolic wave equation with a
source current, $\overrightarrow{J_\perp}$ is

$$\left[\overrightarrow{\nabla_\perp^2} + 2ik\left(\frac{1}{c}\frac{d}{d\tau}\right)\right]E = -\frac{4\pi}{c}\overrightarrow{J_\perp} \bullet \hat{\varepsilon}e^{i\alpha} \quad , \tag{22}$$

where $\overrightarrow{\nabla_\perp^2}$ is the transverse Laplacian with partial
derivatives in the x and y coordinates. The electron
current density $\overrightarrow{J_\perp}$ is the sum of all single-particle
currents,

$$\overrightarrow{J_\perp} = -ec\sum \overrightarrow{\beta_\perp}\delta^{(3)}(\vec{x} - \vec{r_i}(t)) \quad , \tag{23}$$

where $\vec{r_i}(t)$ is the position of the i_{th} electron at time t.
The transverse motion that contributes to the current in
the undulator then reduces from equation (13) to

$$\beta_\perp = \text{Re}(-\frac{K}{\gamma}i\hat{\varepsilon}e^{-ik_o z}) \quad . \tag{24}$$

20

Then combining equations (24) and (23) we obtain

$$\left[\overrightarrow{\nabla_\perp^2} + \frac{2ik}{L}\frac{d}{d\tau}\right]E = -4\pi NeKk\rho(\vec{x},t)dV \ .\qquad(25)$$

To simplify the equation we again introduce $|a|=4\pi NeKL|E|/\gamma_0^2 mc^2$ as the dimensionless laser field, so the complex laser field is $a=|a|e^{i\phi}$, and the dimensionless FEL current density is $j=8\pi^2 Ne^2 K^2 L^2 \rho/\gamma_o^3 mc^2$. Defining dimensionless transverse coordinates as

$$\tilde{x} = x(\frac{k}{2L})^{1/2} \ ,$$
$$\tilde{y} = y(\frac{k}{2L})^{1/2} \ .\qquad(26)$$

We can write the wave equation as

$$\left[-\frac{i}{4}\vec{\nabla}_\perp^2 + \frac{\partial}{\partial\tau}\right]a(\vec{x},t) = -\left\langle je^{-i\zeta}\right\rangle \ .\qquad(27)$$

The Laplacian $\vec{\nabla}_\perp^2$ now involves derivates with respect to the new dimensionless coordinates $\tilde{x}$ and $\tilde{y}$. In equation(27), the $\vec{\nabla}_\perp^2$ terms on the left-hand-side describe diffraction of the beam. When diffraction is small and the electron and optical beam exactly overlap the equation can be rewritten in its simplest form

$$\overset{\circ}{a} = -j\left\langle e^{-i\zeta}\right\rangle \ .\qquad(28)$$

In equation(28), the term on the right is a measure of the bunching of the electrons. The open circle on a is to denote the derivative with respect to dimensionless time as discussed earlier. As seen in equation (17), the evolution of ζ depends on the field a, and we see in equation (28) that the evolution of a depends on the electron bunching, ζ. This is a feedback loop and leads to growth of the

optical field. Eventually, electrons will overbunch and will reach saturation producing no more gain. When $j \leq \pi$ the gain and coupling for the beam will be small and when $j >> \pi$ the coupling and gain will be large.

V.   TRANSVERSE MULTIMODE SIMULATIONS

The three-dimensional oscillator simulations run on a desktop computer. They use the Lorentz force equation for electrons and the paraxial wave equation for light, self-consistently following the evolution of the electrons and the optical wavefront in three dimensions (x, y, and t). Simpler codes only look at the interaction of a single optical mode (i.e., a plane wave) with a relativistic electron beam as it passed through the undulator. The three-dimensional oscillator simulations developed at NPS have the ability to follow multiple transverse optical modes.[4]

The optical field can start with predetermined amplitude and phase or it starts up from noise. In the undulator, the simulation applies the pendulum equation to determine the microscopic motion of the electron in the presence of the undulator and optical fields. It uses the wave equation to consistently update the optical field amplitude and phase. The effects of mirror transmission and edge losses are included. Since the code uses a Cartesian coordinate system, it is not bound to assume axial symmetry and can study the effects of arbitrary shifts and tilts of the electron beam and the cavity mirrors.

In this chapter, we examine the effects of electron beam stability and resulting misalignment. First, we will vary the angle that it enters the optical cavity and then

shift it off axis. We will use both generic FEL oscillator
parameters and the JLab's 14 kW oscillator parameters
results in our study.

A.   GENERIC FEL OSCILLATOR
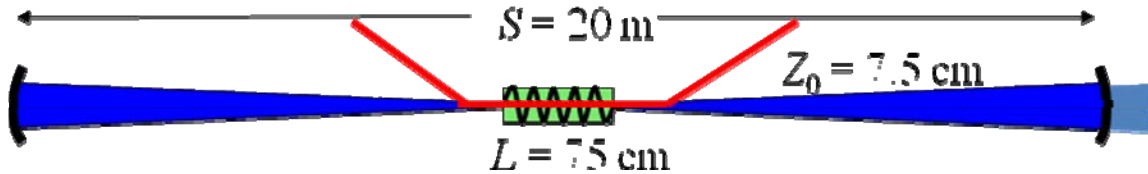
 Figure 7.   Generic FEL Oscillator. Blue represents the
optical field that is bouncing between the two black curved
mirrors. The red represents the electron beam entering the
optical cavity and being steered by magnetic coils to be in
line with the optical mode. The green is the undulator and
    is not shown to scale but enlarged for clarity purposes.

In order to explore the effects of electron beam
misalignments we present the generic oscillator, in Figure
7.   The optical cavity includes all the components that
are between the two mirrors; their operation described in
detail in chapter 2. The optical cavity ~ 20 meters long
while the undulator is only 75 cm in length. The extra
length of the cavity allows for lower intensity light to
impinge upon the mirrors.

Misalignments that cause instabilities can be caused
due to transport path malfunctions. Control systems send
feedback to the magnetic steering components in order to
attempt to place the beam in the correct position. Knowing
the effect of imperfect injection establishes tolerances
that these systems must be designed to. The other factor
that may play a role is vibrations from the platform the
cavity is mounted to.

For the generic oscillator simulations, we fixed the transverse emittance at ε_n = 10 mm-mrad, and the longitudinal emittance at ε_l = 200 keV-ps, corresponding to an energy spread of $\Delta\gamma/\gamma$ = 0.2%. The undulator has 25 periods and the FEL is operates at 1.12 microns. A summary of generic FEL oscillator parameters are in Table 1.

Electron Beam:	
Energy	E_b = 120 MeV
Transverse Emittance	ε_n = 10 mm-mrad
Radius	r_b = 0.1 mm
Longitudinal emittance	ε_l = 200 keV-ps
Bunch Charge	q = 1 nC
Peak Current	I_{peak} = 500 A
Bunch Length	t_b = 2 ps
Energy Spread	$\Delta\gamma/\gamma$ = 0.2%

Undulator:	
Period	λ_0 = 3 cm
Number of periods	N = 25
Length	L = 0.75 m
Undulator parameter	K_{rms} = 1.78

Optical Cavity:	
Wavelength	λ= 1.12 μm
Rayleigh length	Z_0 = 7.5 cm
Cavity Length	S = 20 m
Quality factor	Q_n = 4 (25% loss/pass)

Table 1.   Generic FEL Oscillator parameters.

1.   No Shift or Tilt

We first look at how the generic oscillator behaves with no tilt or shift. Over a hundred passes, we have allowed this FEL to build up to a steady-state optical field. After about 50 passes, the optical mode has reached a relatively stable cross-section shape. At the conclusion of the run, the optical mode has developed a Gaussian intensity pattern at the right-hand mirror. This is shown in Figure 8.

The electron beam started with a relatively narrow energy distribution(recall $\Delta\nu = 4\pi N \Delta\gamma / \gamma$).   After about 50 passes, it has given up energy to the optical field, reached saturation, and begun to overbunch taking some energy back from the optical field, as shown in Figure 9. For this case with no tilting or shifting of the electron beam or the mirrors, the FEL has an extraction of 2.3%.
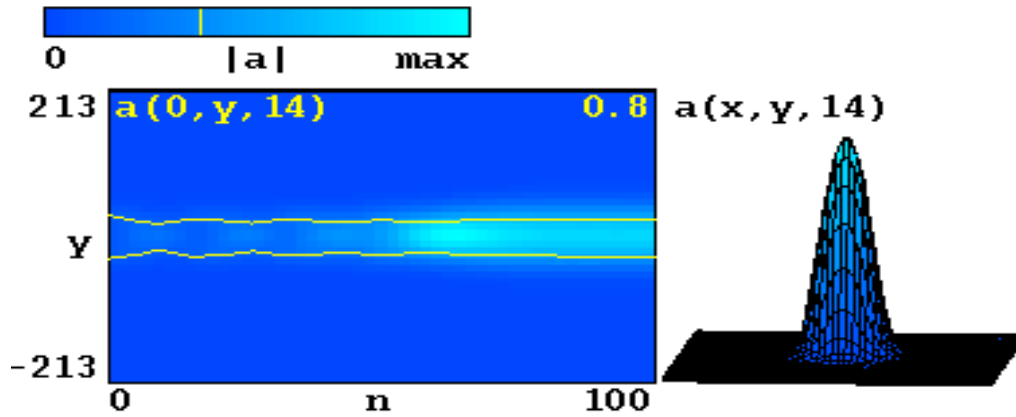
Figure 8.   Generic FEL Oscillator with no tilt or shift. Top left is the color scale for the field amplitude. Bottom left is the evolution a cross-section the optical mode at the right mirror as a function of passes. On the right is the intensity pattern of the optical field at the right mirror.
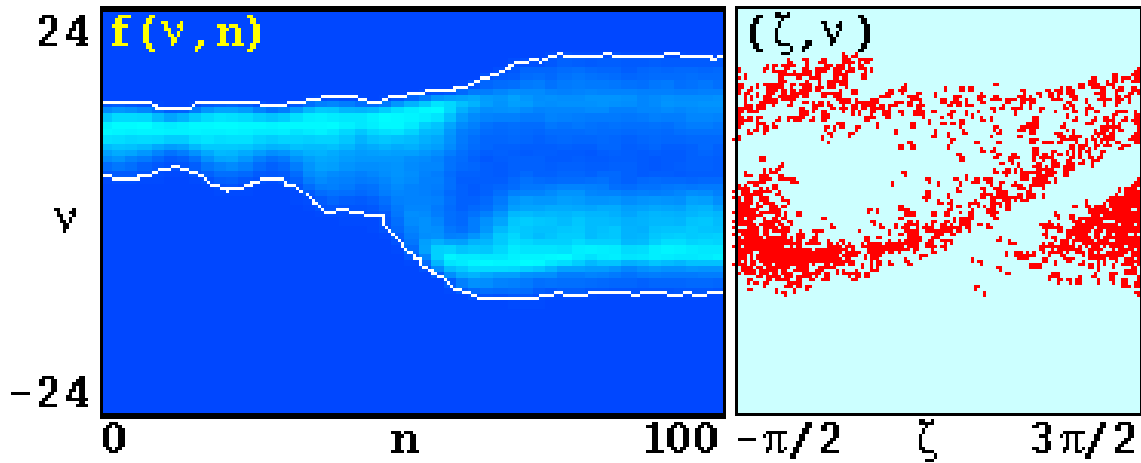
Figure 9.   Left is the evolution of electron phase velocity distribution versus pass number. On the right is the final phase space distribution at the end of the undulator on the last pass in steady state.

2.   Electron Beam Shift

The electron beam will now be shifted off axis from 0 to 1.5 mm. It no longer passes through the center of the cavity where the energy exchange between the optical field and electron beam would normally be taking place. A cross section of the electron beam and the optical field on the last pass through the undulator is shown in Figure 10. Three different scenarios are shown: an electron beam shift of 0, 0.5 and 1.5 mm (from top to bottom). The simulation handles about 30,000 electrons so what is shown in red is only a small sample in order to visualize their position. The spacing from how many integration time steps were taken through the undulator. In this case, we used 50 time steps

In the 0.5 mm shift case, the electrons are amplifying the optical field off axis more than on axis and the optical field mode at the waist pulled upwards. Since the optical field strikes the upper part of right-hand mirror it is reflected at an angle, causing the mode to pivot about the middle. In the drastic case of 1.5 mm shift, the optical mode is steered by the interaction and FEL power is reduced.

The yellow curve at either end of the undulator represents a cross-section of the optical field. It can be seen that the optical field has moved off axis substantially compared to the fundamental Gaussian mode shown in magenta.

There is no evidence of any betatron oscillations in Figure 10. The betatron oscillations would tend to focus the electron beam to keep it on axis in the undulator

28

causing a sinusoidal pattern in the red dots. The betatron frequency in an undulator is given by [4]

$$\omega_\beta = 2\pi \frac{NK}{\gamma} \quad .$$ (29)

where N is the number of periods, K is the undulator parameter and γ is the Lorentz factor, all as discussed in the theory section. For this case, $\omega_B = 1.2$ so we would expect about 1/5 of an oscillation over the length of the undulator, $\tau=0->1$. There should be very little apparent focusing, as the simulation shows.

One consequence of a shift of the electron beam is that the optical field would leave the optical cavity at an angle that would have to be accounted for in the beam control system. This angle of exit could be an important issue for control systems, even if the system is still performing at an adequate extraction level.
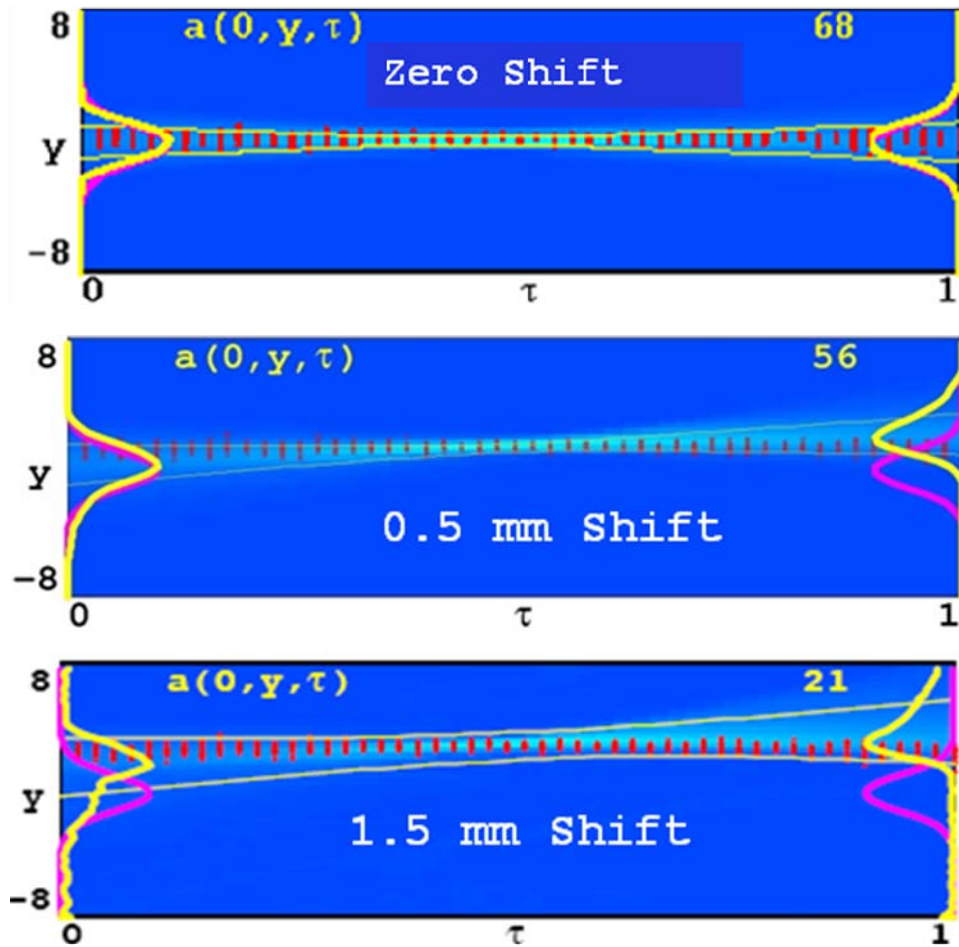
Figure 10.   Cross section of electron beam and optical field as it progresses from τ = 0->1 on the last pass through the undulator. In red are sample electrons. In blue is the optical field, using the same color scale as before. The thin yellow lines indicate the 1/e points of the optical field amplitude. The thick yellow lines on the left and right are cross-sections of the optical field amplitude at the beginning (τ=0) and end (τ=1) of the undulator. They are overlaid onto the magenta curves, which correspond to the fundamental Gaussian mode for the cavity. The top picture is with no tilt or shift. The center picture is for an electron beam shift of 0.5 mm, and the bottom picture is for a shift of 1.5 mm.

Another useful feature of the simulation output is to be able to look at what is happening with the optical field and its mode composition at the right mirror of the cavity. The progression of a shift of 0-2.7 in dimensionless units, as described in chapter 2, is shown in Figure 11. The shifts correspond to a range of 0-1.5 mm. Recall from chapter 2: the black lines just outside the border of each window on the right and lower boundaries represent the extent of the mirrors modeled. In the generic oscillator case, the mirrors extend all the way out to the edge of the optical window, so there is no leakage outside the mirrors, even for large tilts and shifts. In yellow is the optical field profile at the mirror on the last pass of the simulation. At higher electron beam shifts it becomes evident that the mode make up is distorted and the physical location that the peak field hits the mirror is also off axis.

We see that the electron beam is trying to pull the light off axis. However, the peak of the optical field is not necessarily shifting off axis proportional to the electron beam shift, as seen in Figure 11. This is due to the competition between the fundamental Gaussian mode cavity is and the gain that the electron beam is providing off axis. Consequentially, there is broadening in the optical field vertically corresponding to the electron beam shift along this axis.
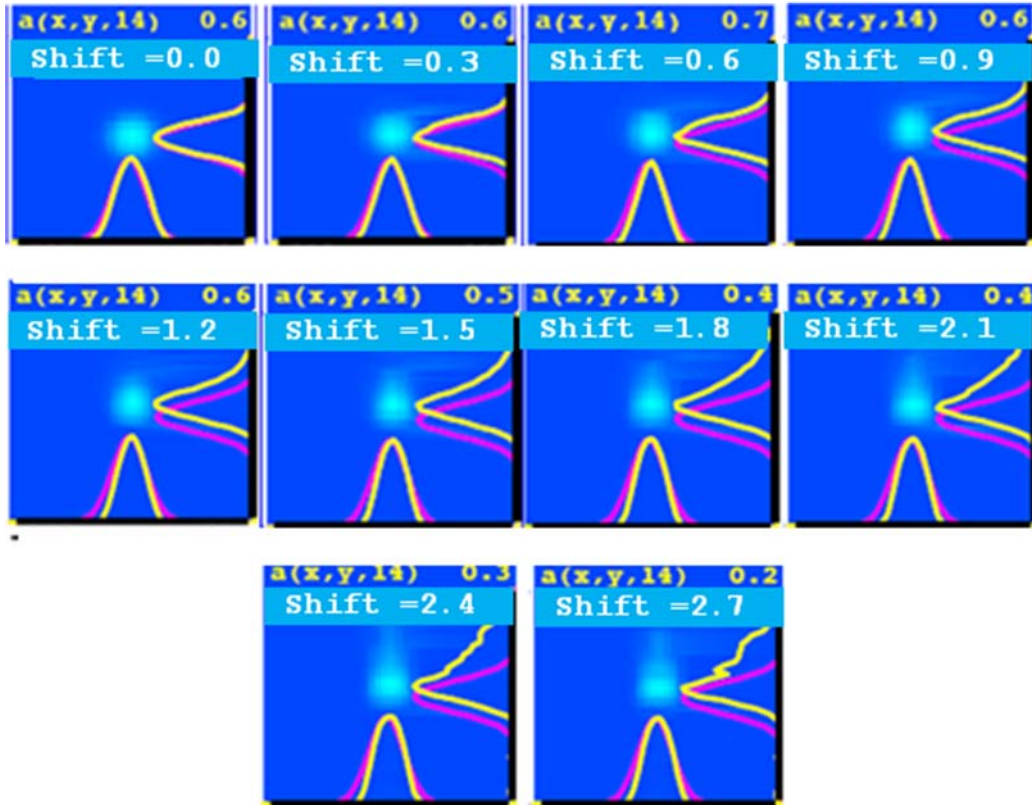
Figure 11. Optical field at mirror. Specifically, the partially transmissive mirror on the right side of the cavity. Ten cases showing the evolution of the optical field as a function of electron beam shift. The shift values shown are dimensionless and correspond to a range of 0-1.5 mm shift in electron beam off axis.

3.   Electron Beam Tilt

Electron beam tilt can occur because of component vibrations or equipment misalignment. Typical vibrations in the system are of acoustic frequencies on a much longer time scale than the round-trip time of the optical pulses, so the effect on the FEL interaction is modeled as a static tilt. The incoming electron beam is tilted as it enters the optical cavity from zero to 8 mrad and the effect on the FEL performance is analyzed.

Two amounts of tilt in the electron beam are presented in Figure 12. For reference, the non-tilted case is shown with two increasing degrees of tilt following beneath. In the middle example, the shift is about 5 mrad resulting in an extraction of about 2 percent. However, one can see at the left end of the undulator, that higher order modes are amplified as evidenced by the distortion in the shape of the optical field as compared to the Gaussian.

The lower picture shows a decoupling of the optical beam and the electron field for most of the undulator and thus there is very little bunching of gain. The extraction is essentially zero. Note that the peak optical field amplitude indicated in yellow in the upper right is much smaller than the other cases (~10-6). The optical beam is trying to follow the electron beam as the tilt increases. The cavity, at the same time, is competing by trying to sustain its fundamental Gaussian mode, determined by the cavity length and mirror curvature. In the lowest picture, the FEL is not working and the power is headed to zero.

33
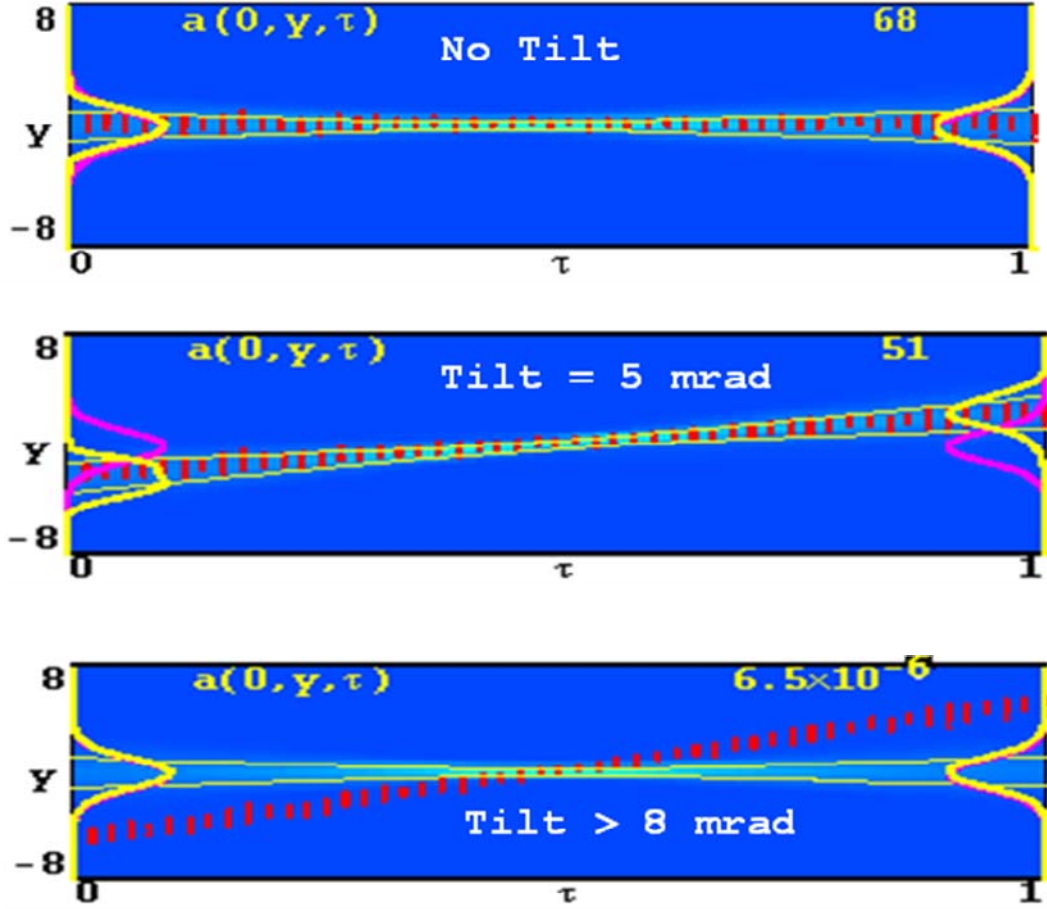
Figure 12.   Electron beam tilt. Top is no tilt followed by a tilt of 5 mrad (middle) and then a tilt in excess of 8 mrad (bottom).

A series of figures of the optical field at the right mirror as we vary the electrons beam tilt is shown in Figure 13.   There is a dramatic difference in the optical mode shape at the mirror as the tilt is increased. Although the goal was to make the mirrors large enough so that mirror edge losses did not contribute to loss, we see there is still the largest decrease in performance when the optical field starts to "leak" out the top edge of the mirror.   In order to avoid this, the study would have to be performed with even larger mirrors.

The amount of tilt tolerated by the operating FEL is known to be much more than with a comparable "cold" cavity [6]. The FELs directional gain medium, the electron beam, works to keep the cavity mode aligned.
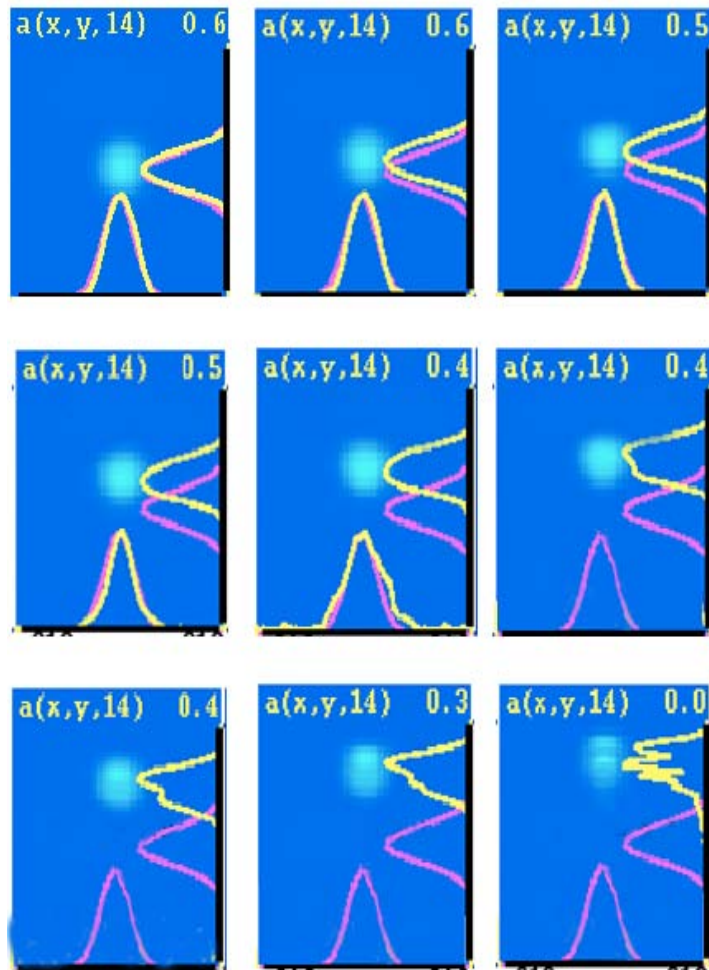
Figure 13. **Optical field at right mirror as a function of tilt.**

4.   Combined Effects on Extraction

For the generic oscillator we have looked at various aspects of the operation during electron beam misalignments. One of the key parameters to report however is the extraction as a function of both the electron beam tilt and shift, as shown in Figure 14. On the right is a color scale for the extraction.

In the previous pages, we have shown that there is a difference in sensitivity for FEL beam shifts or tilts. Specifically when we were shifting the electron beam there was a consistent gradual degradation in performance. However, when tilting the electron beam a critical angle was reached past which the degradation was distinct. The large difference between the two scenarios is that while in the shift cases we presented the overlap between the electron beam and optical field existed along the whole undulator, in the most extreme tilt cases, the electron beam and optical field were decoupled.

For the generic oscillator we find that to get an extraction of greater than 1% we need a beam with a combined shift and tilt of less than 0.6 mm and 4 mrad, respectively.
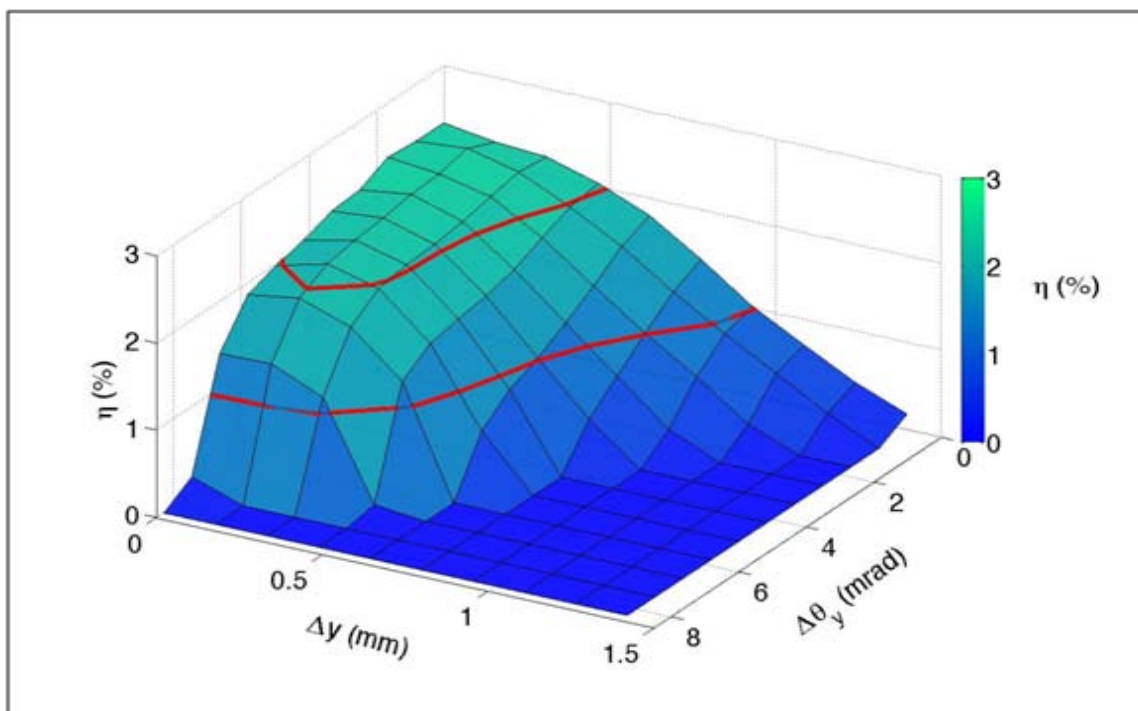
Figure 14. Extraction (η) versus both electron beam shift (Δy) and electron beam tilt ($\Delta\theta_y$). The red contour lines correspond to extractions of 1 and 2%.

B.   JEFFERSON LAB FEL OSCILLATOR

We next explore the effects of electron beam and mirror tilt and shift in an existing experiment.   In October of 2006, the Jefferson Lab (JLab) FEL achieved a record average power of 14 kW. JLab utilizes an energy recovery linac in order to increase the overall efficiency of the machine.   This is similar to what the Navy intends to do with their laser weapon in order to increase the efficiency and decrease the energy of the electrons at the beam dump, as described in chapter 1.

A schematic of the JLab experiment is shown in Figure 15.   In orange is the injector, the red arrows show the accelerating   electrons,   the   blue   arrows   show   the recirculating electrons coming back into the accelerator in such a RF phase that they give energy back.   They are steered to an energy dump for disposal.   The optical cavity, circled in red, is the region that we will simulate the interaction.

The cavity length is 32 m long (the generic oscillator was 20 m) and the undulator length is 1.65 m (vice 0.74 m studied previously).   The core bunch charge is only 0.114 nC (much lower than 1 nC for the generic oscillator.)   The transverse emittance of ε_n = 8 mm-mrad is comparable, however, the JLab longitudinal emittance is substantially lower at 80 kev-ps, corresponding to an energy spread of $\Delta\gamma/\gamma$ = 0.4 %.   This is mainly due to the much lower bunch charge.   The undulator has 30 periods and the optical cavity is designed for a wavelength of 1.6 microns.   The parameters are summarized in Table 2.
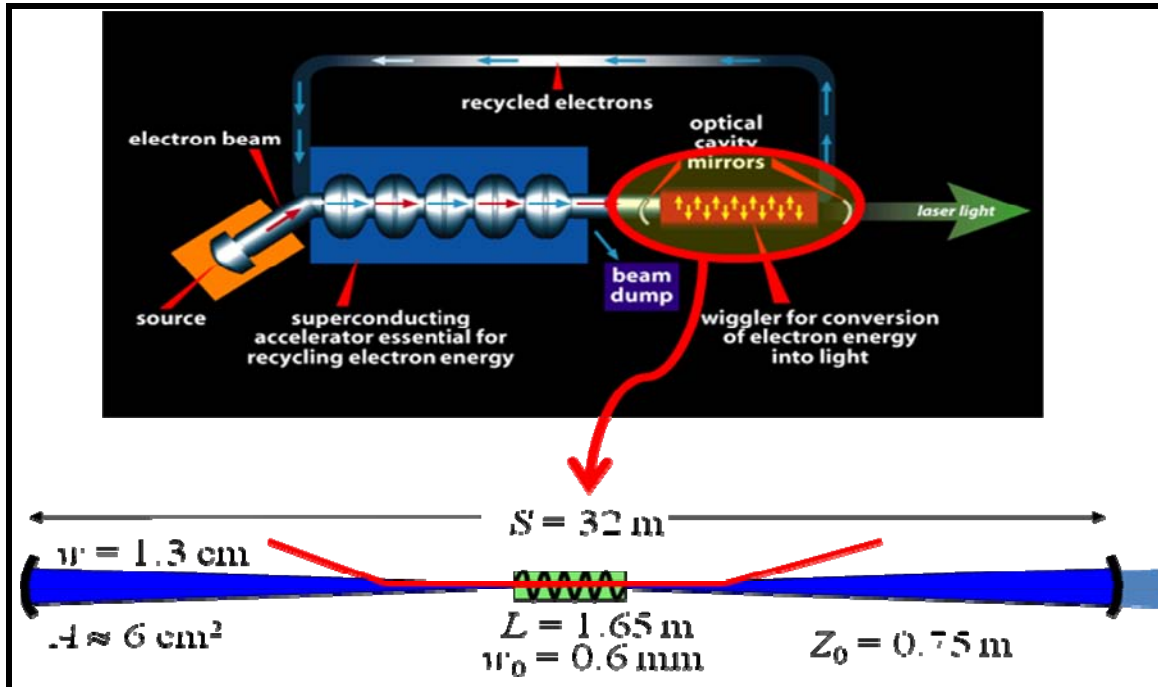
Figure 15.   Schematic of the Jefferson Lab FEL
Oscillator. Shown is both the overall system including the
recirculation path for electrons and then a blown-up
picture of just the optical cavity. [From 5].

Electron Beam:	
Energy	E_b = 115 MeV
Transverse Emittance	ε_n = 8 mm-mrad
Radius	r_b = 0.17 mm
Longitudinal Emittance.	ε_l = 80 keV-ps
Bunch Charge	q = 0.114 nC
Peak Current	I_{peak} = 285 A
Bunch Length	t_b = 0.4 ps
Energy Spread	$\Delta\gamma/\gamma$ = 0.4%

Undulator:	
Period	λ_0 = 5.5 cm
Number of periods	N = 30
Length	L = 1.65 m
Undulator parameter	K_{rms} = 1.36

Optical Cavity:	
Wavelength	λ= 1.6 μm
Rayleigh length	Z_0 = 75 cm
Cavity Length	S = 32 m
Quality factor	Q_n = 5

Table 2.   JLab Oscillator parameters.

1.   No Shift or Tilt

We begin by looking at how the JLab experiment operates with no misalignments. The number of passes is increased to 200 from the 100 used for the generic oscillator, but the optical mode again has stabilized after about 50 passes, as shown in Figure 16. The electron phase space distribution on the right shows that the electrons have bunched and reached saturation and the optical mode shape in the middle is a Gaussian shape.
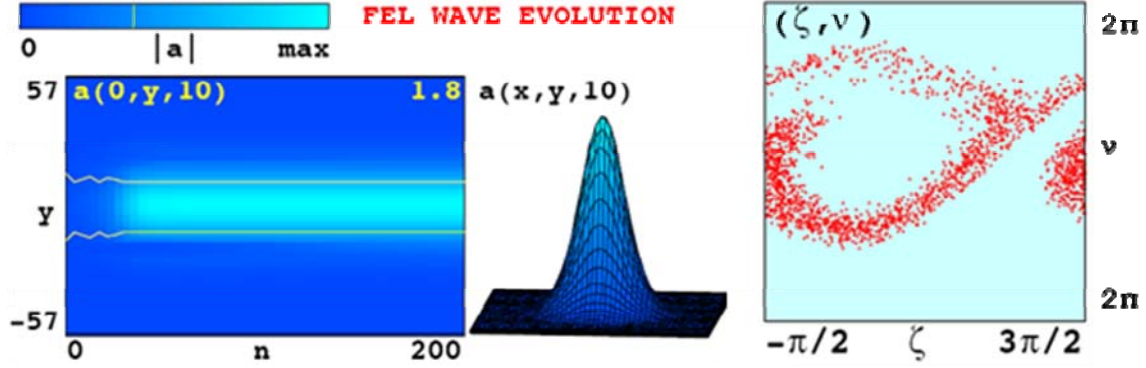
Figure 16.   JLAB oscillator with no misalignments in the electron beam or mirrors. On the left is the evolution of the optical mode, as a function of the passes. The optical field at the right mirror on the last pass is in the middle. On the right is the electron phase-space plot at the conclusion of the last pass.

The power and gain evolution as a function of passes is shown in Figure 17. In the actual experiment, the machine will start up from noise but in our simulation, we start from a small source of initial light in the cavity. The resulting steady-state solution at saturation is independent of the initial field. The extraction reached is 2%, which corresponds to 20 kW of output power through

the 20% transmissive right mirror. Since the electron
pulse length is slightly less than three times the slippage
distance, we would expect pulse slippage to mildly affect
the results. Based on 2D simulations, had we taken these
into account we would have found about a 20% decrease in
extraction, which would have resulted in an average optical
power of 16 kW, close to the observed 14 kW.

The optical field at the partially transmissive mirror
is shown on the right of Figure 17. The 1/e width of the
electric field amplitude is approximately 14 mm, which
compares well with experimental results. The thick black
lines on the right and lower edges of the picture represent
the mirror as before. In the case of JLab, there is not as
much space for the optical field to shift before the edges
of the mirror will be reached. It is expected that this
will affect the sensitivity to shift and/or tilts.
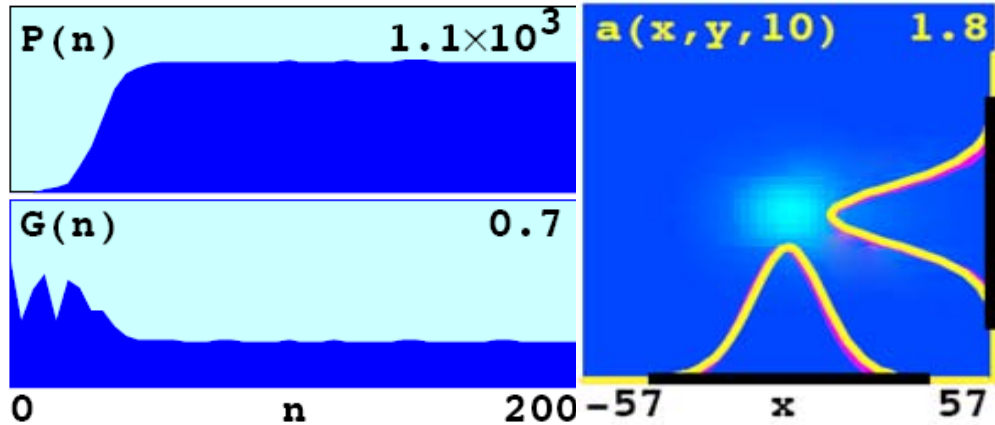
Figure 17.   **Top left is the power evolution and the
bottom left is the gain evolution for the JLab FEL
oscillator. Both are a function of number of passes, *n*=0-
>200 for this oscillator. On the right is optical field at
the right mirror, which is aligned well with the
fundamental Gaussian mode.**

2. **Electron Beam Shift**

The electron beam was shifted off-axis from 0 to 2 mm. Recall that for the generic oscillator we shifted from 0–1.5 mm. The electron beam and optical field in the undulator on the last pass in steady state are shown in Figure 18. On the right is the corresponding 3D rendition of the optical field at the right mirror. The unshifted case is presented on the top followed by the 0.55 mm and then the 1.1 mm shift results. The extraction for these three cases for comparison is 2.0%, 1.6 % and 0.5%, respectively.
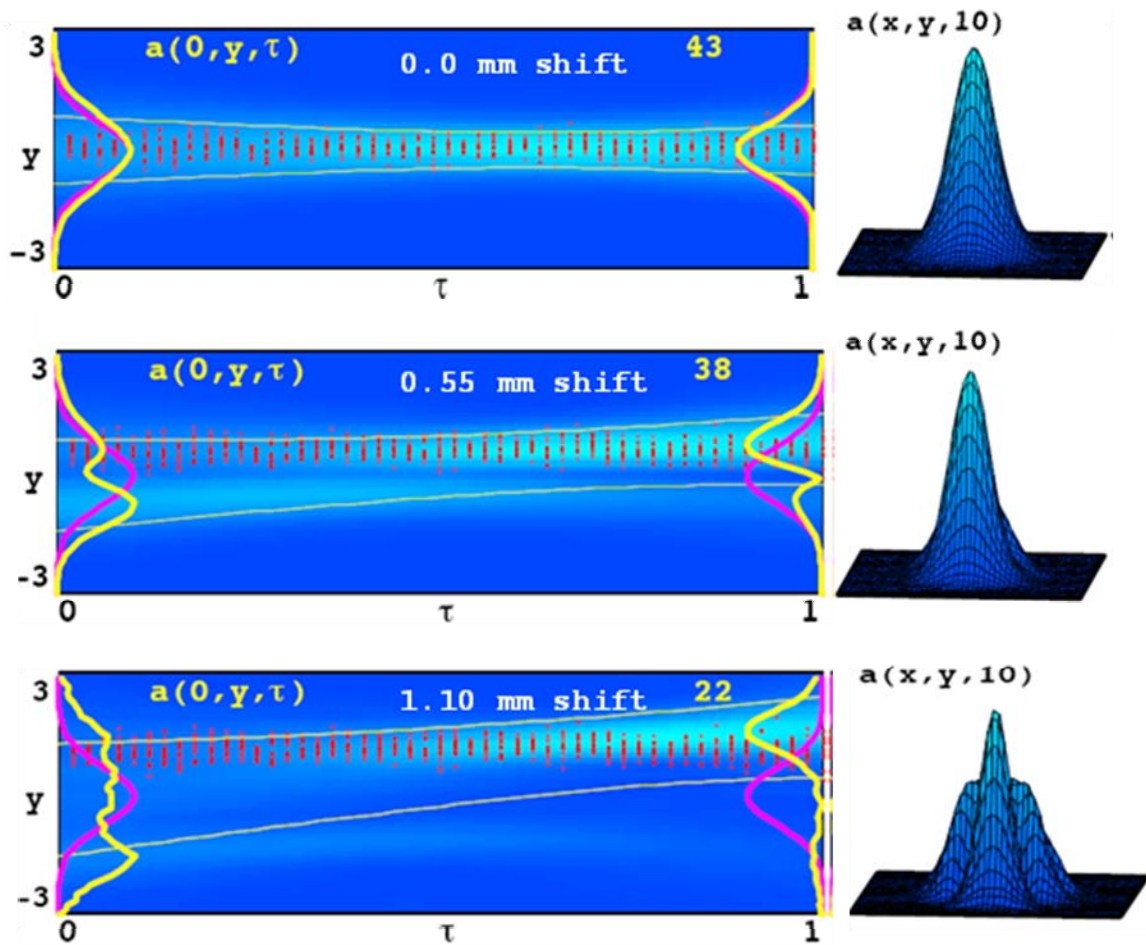
Figure 18. JLab FEL oscillator with various electron beam shifts. From top to bottom are 0, 0.55, and 1.1 mm shift off axis. On the left is the cross section of the electron beam and the optical field as it progresses from τ=0->1 in dimensionless time through the undulator on the last pass. On the right is the optical field at the right mirror after the final pass.

The mirror size is affecting the tolerance to electron beam shift in Figure 19. Mirror edge losses occur as early as in the 0.44 mm shift, which is the top right picture in Figure 19. When the light starts clipping at the edge of the mirror there is an increasing amount of diffraction pattern in the optical field. It further intensifies the higher-order mode composition of the optical mode. In order to keep the extraction greater than 1%, we find the beam should not shift more than 0.75 mm. This corresponds to the third picture from the left in the bottom row of figure 14. A good portion of the optical mode now is outside the Gaussian and the peak has been shifted by about a quarter of the Gaussian fundamental mode width. The overall performance as function of the shifts is presented along with the tilt data in the next section.
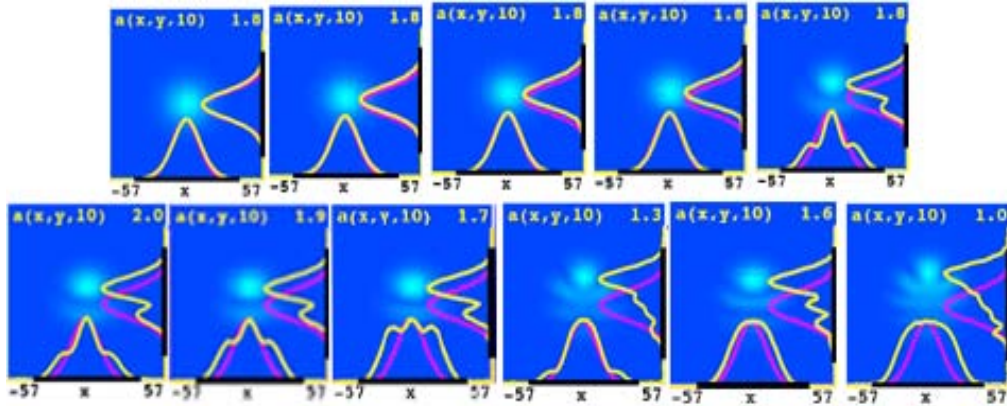
Figure 19.   The right mirror and is associated optical mode and position. The electron beam is being shifted on axis in progression from left to right top to bottom. The range covered is 0 – 1.1 mm total shift in equal increments.

3.   Electron Beam Tilt

Various ranges of electron beam tilt were examined for the JLab experiment in order to bracket the amount of tolerable tilt in the range of 0-4 mrad. To compare the JLab experiment to the generic oscillator, we can look at how both performed in the range between 0 -> 1 mrad electron beam tilt. In the case of the generic oscillator, the extraction decreased about 3% of its original value. However, the JLab experiment's extraction decreased by roughly 18% of its original value for the same tilt. This can be attributed to two effects, seen in Figure 20. On the top is the generic oscillator's electron beam and optical mode field as it passes through the undulator. Beside it is the optical field at the right mirror. Below is the same for the JLab oscillator. (i) Notice that the generic oscillator has more of a peak shift at the mirror than JLab. This is because the light is "following" the electron beam tilt for the generic oscillator, but not for JLab. (ii) Also notice that the electrons in the undulator are physically staying within the 1/e width (thin yellow line) of the optical field for the whole distance of the undulator for the generic case, but not JLab. This is vital for the gain of an FEL. The conclusion is that the generic oscillator is less sensitive to electron beam tilt than JLab.

Due to its shorter Raleigh length, the mode diverges more rapidly for the generic oscillator, as shown in Figure 20. This agrees with published results [6] that concluded that as electron beam is tilted it is still able to overlap with the optical field and provide gain.
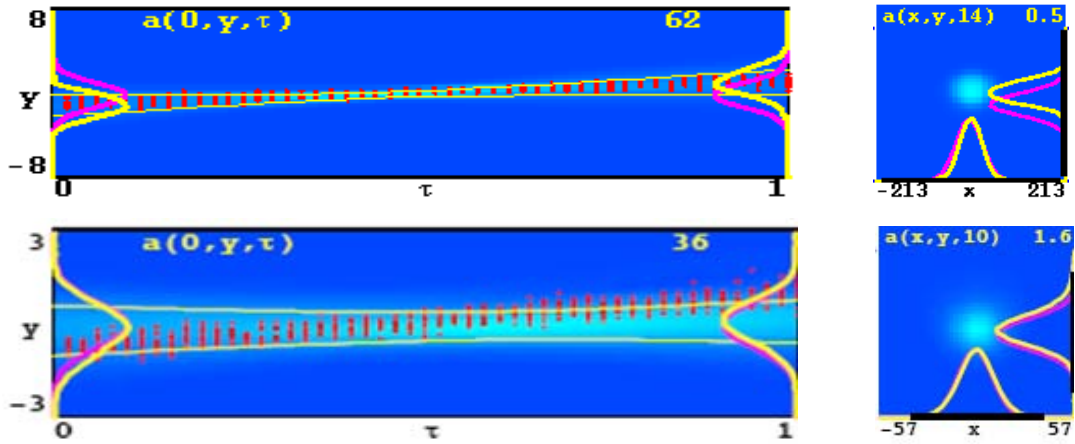
Figure 20. Generic oscillator electron beam and optical field in the undulator (top left) and the optical field at the right mirror (top right). On the bottom is the same for JLab oscillator experiment for comparison.

4. JLab Extraction

The extraction as a function of electron beam shift is shown in Figure 21. The extraction as a function of electron beam tilt is shown in Figure 22. Included with the graphs are figures showing the optical modes for specific values. There is a 50% drop in extraction if the beam is shifted by $\Delta y \approx 0.8$mm. The electron beam tilt for the same fractional drop in extraction is $\Delta \theta_y \approx 1.2$ mrad. The extraction of the generic oscillator drop by 50% at a similar shift of about 0.8 mm, but a much larger tilt of about 7 mrad. The JLab experiment is much more sensitive to tilt in the electron beam than the generic oscillator. We believe this is due to its longer Raleigh length, ant to the optical power clipping by the mirror edges.
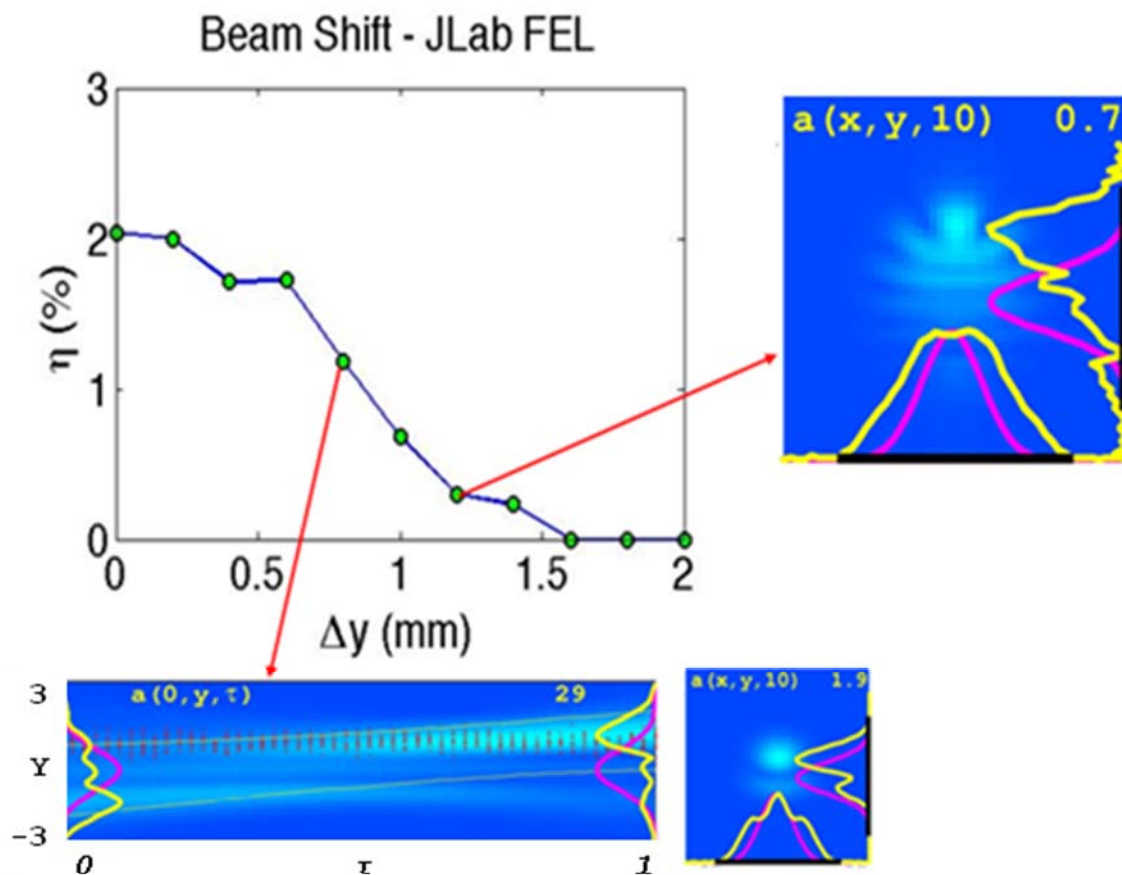
Figure 21.   Extraction as a function of electron beam shift for the JLab FEL oscillator. Included is electron beam and optical field plots at the partially transmissive mirror and along the undulator.
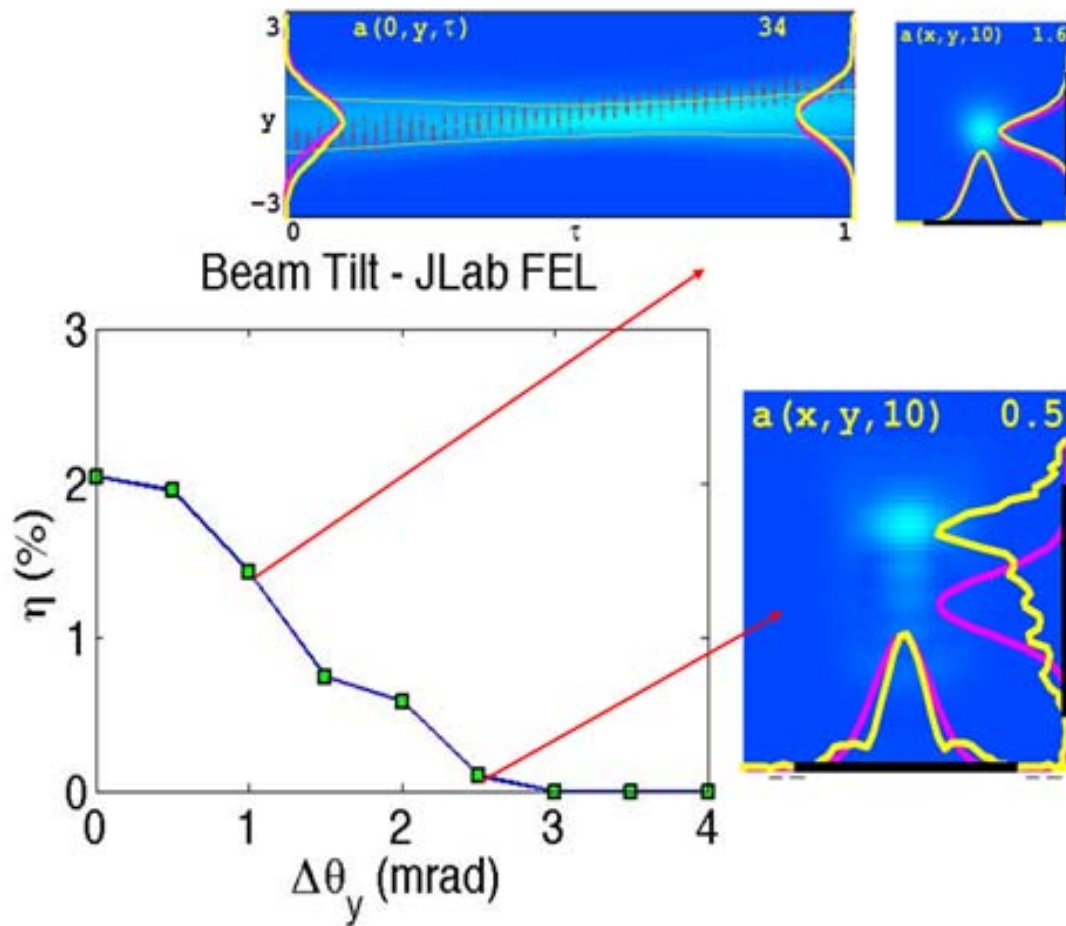
Figure 22. Extraction as a function of electron beam tilt about the center of the undulator for the JLab FEL oscillator. Included are electron beam and optical field plots at various points.

THIS PAGE INTENTIONALLY LEFT BLANK

VI. FOUR-DIMENSIONAL SIMULATIONS

The four-dimensional (4D) amplifier simulation runs on a cluster computer. It similarly uses the Lorentz force equation and the paraxial wave equation self-consistently following the evolution of the electrons and the optical wave. Instead of just following the optical wavefront as described for the transverse multimode simulation, the 4D simulation slices the optical pulses up into sections, so that each node of the cluster follows one slice of the pulse. The NPS 128 node cluster is shown in Figure 23. It can handle approximately 100 slices of the optical pulse shown in A typical simulation includes about three million electrons. Since the electrons are traveling slightly slower than the optical pulse, they will continually "slip" back, lagging the optical pulse. To account for this slippage the sample electrons continually pass from one node to the next at appropriate intervals of time [4].

The left two pictures show the relative position of the electrons (in red) to the optical pulse (in blue) at the beginning and end of the undulator. Recall that τ is the dimensionless parameter for time, which varies from zero to one, from the beginning to the end of the undulator. At the beginning of the undulator, $\tau=0$, the electron pulse (in red) is ahead of the optical pulse (in blue). As time progresses the electrons slip back continuously. The difference in the optical field from $\tau = 0$ to 1 is due to the gain process. The pulse width narrows and its peak shifts as the electrons slip back and amplify only the portion of the optical field that they pass over.

51
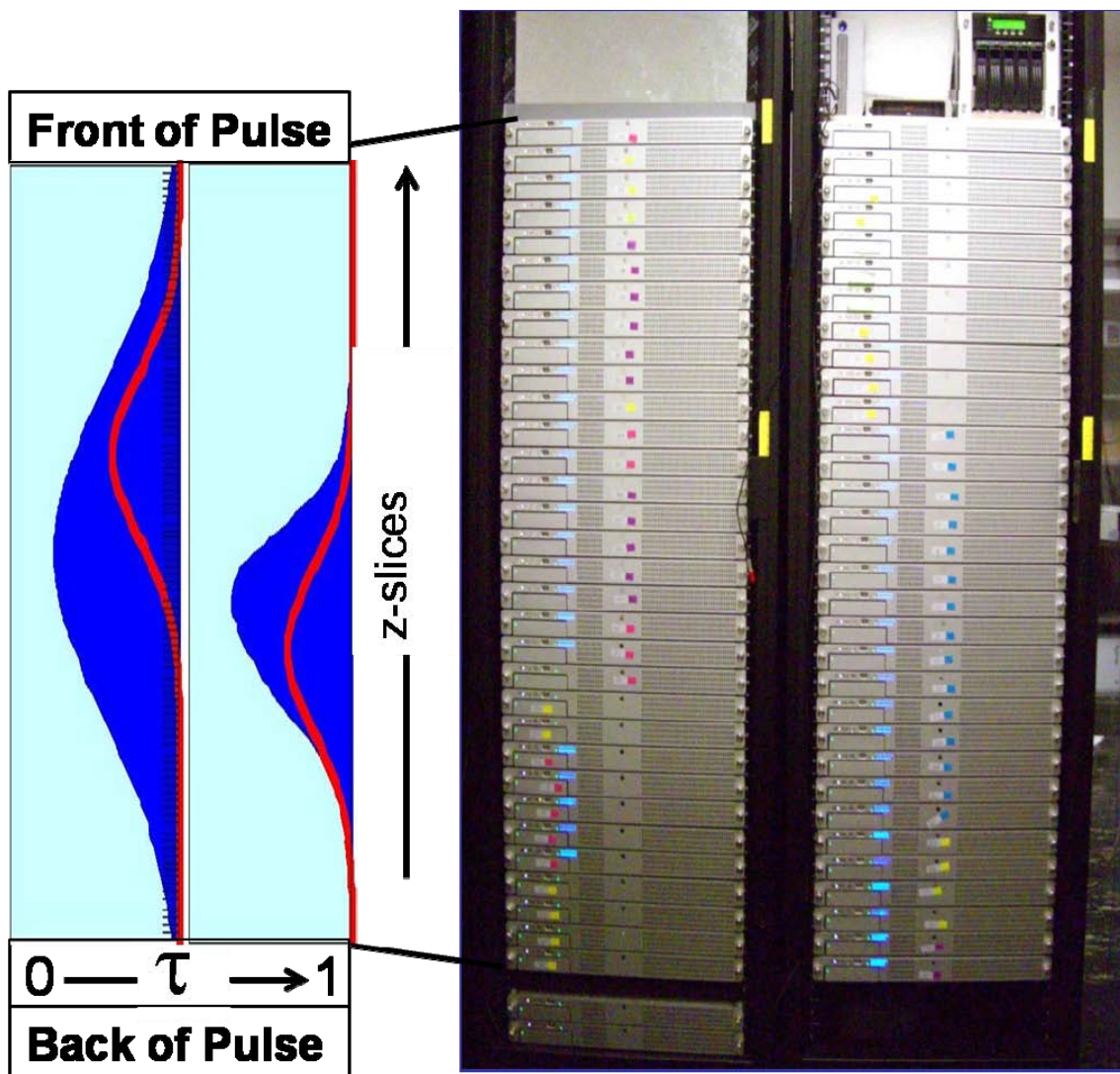
Figure 23.   NPS 128-processor Apple Xserve cluster.
Contains 64 nodes and is used to simulate FELs in x,y,z and
t. On the left are two pictures showing the relationship
between the electron pulse, in red, and the optical pulse,
in blue. The two pictures are from the beginning ($\tau=0$) to
the end ($\tau=1$) of the undulator.

A.   GENERIC FEL AMPLIFIER

The generic amplifier simulated has many parameters that are similar to the generic oscillator presented earlier. A schematic is provided in Figure 24.
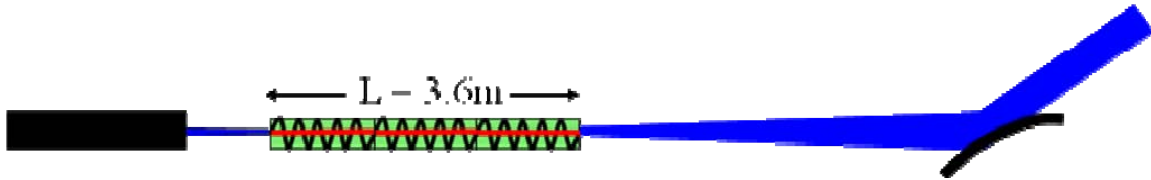
Figure 24.   Generic FEL amplifier basic layout. In red is the electron beam. In Blue is the optical field. In green is the Undulator. On the left in black is the seed laser and on the right is the first optical mirror that the optical field will meet.

We used the same electron beam and undulator parameters as before with the exception of the undulator length.   The length is approximately five times larger increasing from 75 cm to 3.6 m.   In the oscillator configuration, the light is stored in the region between the mirrors and its amplitude allowed to build up over many passes. In the amplifier, there is only one pass for the light to reach a useful power level. For this reason, the length of the amplifier undulator is much longer than the oscillator to achieve the necessary gain and energy extraction.

The transverse multimode simulations started from a weak initial optical field. In an FEL amplifier, the seed laser determines the initial optical field. The electron beam energy is 120 MeV with a bunch length of 2 ps. The undulator has a period of 3 cm and is 3.6 m long. The seed laser has an optical power of 1 watt, wavelength of 1.11 μm and pulse length of 4 ps. The parameters of the generic

amplifier are given in Table 3. We will use the 4D simulation code to describe the performance of the generic amplifier as a function of electron beam tilt and shift.

Electron Beam:	
Energy	E_b = 120 MeV
Transverse Emittance	ε_n = 10 mm-mrad
Radius	r_b = 0.3 mm
Longitudinal Emittance	ε_l = 200 keV-ps
Bunch Charge	q = 1 nC
Peak Current	I_{peak} = 500 A
Bunch Length	t_b = 2 ps
Energy Spread	$\Delta\gamma/\gamma$ = 0.2%

Undulator:	
Period	λ_0 = 3 cm
Number of periods	N = 120
Length	L = 3.6 m
Undulator parameter	K_{rms} = 1.8 (1cm gap)

Seed Laser:	
Wavelength	λ= 1.11 μm
Average Power	P_{opt}=1 W
Pulse Length	t_{opt} = 4 ps
Peak power	P_{peak}=330 kW

Table 3.   Parameters of the generic amplifier.

54

1.   Electron Beam Shift

The electron beam is shifted off the undulator axis by 0 to 1 mm.   A side and top view of the optical field and electron beam in the undulator are shown in Figure 25.   The optical field in light blue is shown to grow as it interacts with the electron beam and reaches maximum field strength at the end of the undulator.   The electron beam has a shift off the undulator axis by Δy = 0.4 mm and no tilt.   The sampled electrons in red are shown to be steered toward the axis in the lower picture by the betatron oscillation.   Equation(29) predicts that there will be about 0.9 betatron oscillations in the undulator, which agrees with the simulation.   At the end of the undulator, the electron beam is off-axis by approximately the same amount when it entered the undulator.   To the right of the bottom picture, the cross section shows the electron beam (red) overlapping the peak of the optical field (blue). This overlap will affect the FEL performance.
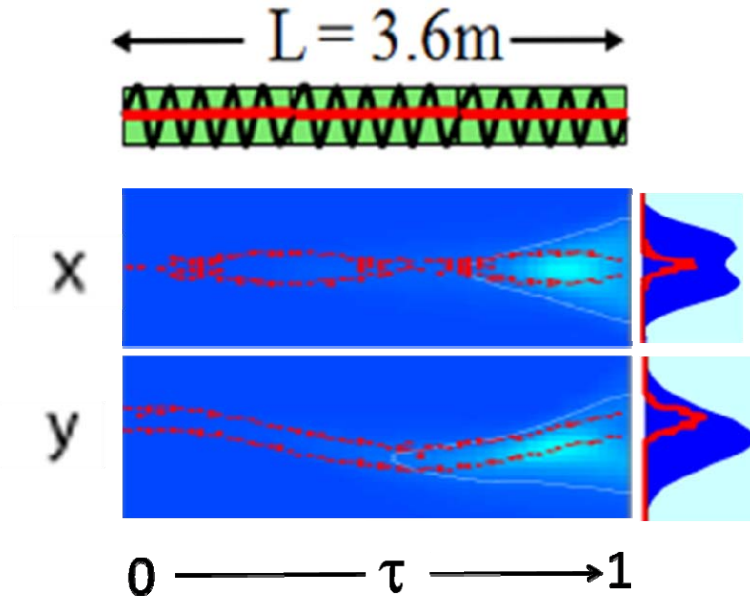
Figure 25.   Generic FEL amplifier, showing the electron beam (red) and optical field (blue) as they progresses from τ = 0->1.   In red are sample electrons.   The electron beam was shifted by 0.4 mm in the y direction.   To the right of each picture are cross-sections vs. x and y of the electron beam and optical field.

The optical field at both the end of the undulator and the first mirror are shown on the left and right of Figure 26.   There are higher order modes that have developed shown by the yellow curves that represent the optical field. Unlike the oscillator, the optical field is still on axis. This   can   be   contributed   to   the   betatron   oscillations bringing the electron beam back on axis for the last part of   the   undulator,   which   also   is   where   the   most   energy exchange occurs.   The extraction for this shift of 0.4 mm is 0.5%, half the value optimal achieved with no shift or tilt in the electron beam.
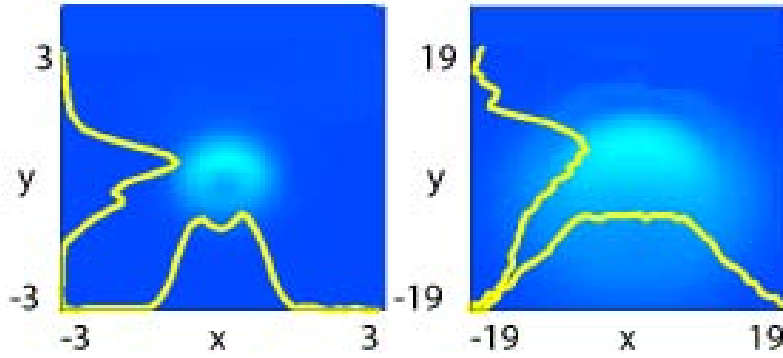
Figure 26.   Generic Amplifier, optical field at the end of undulator (left) and first mirror (right). The yellow curves are cross-sections of the optical field.

2.   Electron Beam Tilt

The electron beam is now tilted when it enters the undulator by 0 to 1 mrad. The generic amplifier with the electron beam tilted in y by 0.4 mrad as it enters the undulator is shown in Figure 27. Again, betatron oscillations bend the electron paths toward the undulator axis. The overlap along the undulator is not very much different when looking at the tilt and shift cases.
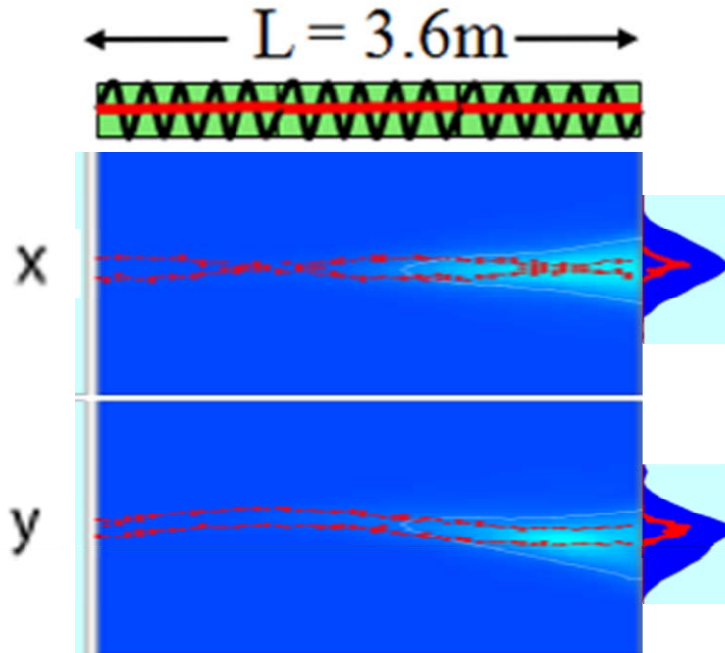
Figure 27.   Generic amplifier with the electron beam
entering at a 0.4 mrad tilt about in y.

3.   Combined Effects

The electron beam was shifted and tilted over all
combinations of the ranges that were previously discussed.
The Extraction is plotted in Figure 28.

The generic FEL amplifier decreases down to 50% of the
maximum extraction for an electron beam shift $\Delta y \approx 0.4$ mm
and tilt, $\Delta \theta y \approx 4$ mrad.   The generic oscillator had a
similar 50% drop in extraction for shift $\Delta y \approx 1$ mm, tilt $\Delta \theta y$
≈ 7 mrad.   Since the machines are as similar as possible,
it is found that the generic amplifier is more sensitive to
electron beam shifts and tilts than the generic oscillator.
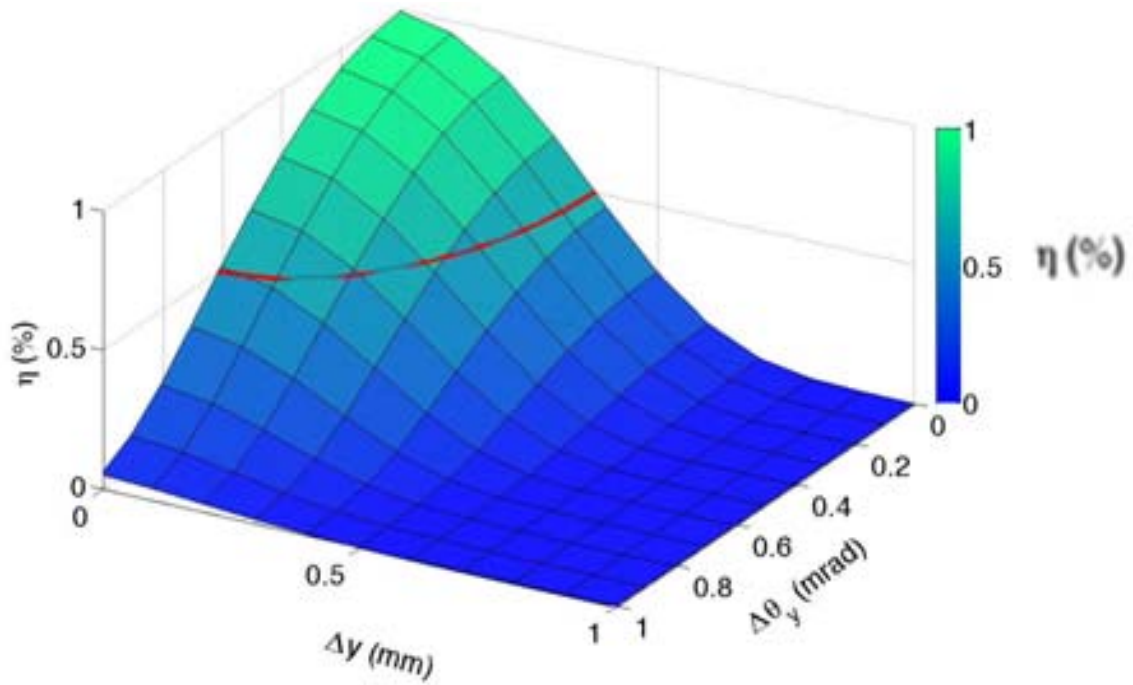
Figure 28. Generic Amplifier extraction as a function of both shift and tilt of the electron beam. At the peak value, there is an extraction of just over 1%. The red line corresponds to an extraction of 0.5%.

THIS PAGE INTENTIONALLY LEFT BLANK

VII. ELECTROSTATIC CATHODE TEST CELL

As discussed in Chapter II, the first component in the FEL is the injector where electrons are extracted from a surface, the cathode, and an electron beam created. The beam quality out of the injector is usually the best that we can have anywhere in the system. The NPS FEL group is beginning its cathode research using the original DC gun-based injector system from the Stanford Superconducting Accelerator (SCA). A schematic of this 2 stage, 240 kV DC gun is shown in Figure 29. It has Pierce-type geometry and a gridded cathode.

When first emitted, electrons have negligible velocity of just a few eV. The space charge effects, due to many charged particles being in close proximity, cause the beam to diverge. Pierce geometry provides initial focusing by angling the cathode surface to curve equal potential lines just outside the surface. Since the electrons are governed by the Lorentz force equation described in Chapter II, they will tend to travel perpendicular to such equipotential lines along electrostatic field lines. As such, this Pierce-type geometry tends to focus the electron beam helping to counter the defocusing effects of space charge.

The SCA gun is currently being used for low-energy beam transport studies and cathode characterization. Based on the current configuration, with a potential difference of 100 kV, the gradient at the cathode center is 1.4 MV/m. The maximum radius of the cathode in this design is 4 mm based on the inner radius of the Pierce-type electrode ring.
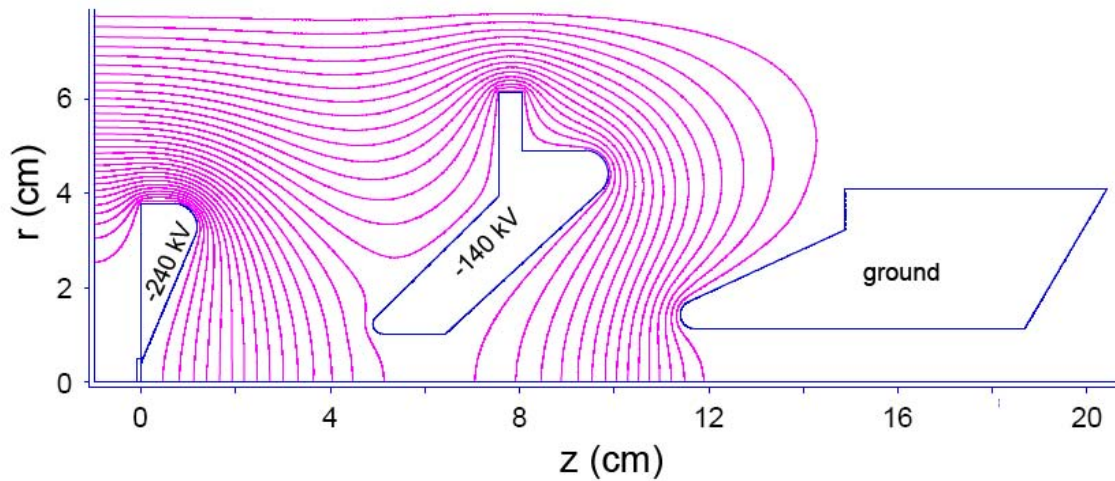
Figure 29.   Original DC gun from Stanford Superconducting Accelerator (SCA). This figure shows the DC Gun electrode geometry and equipotentials (in magenta). [From 7]

A.   FIELD EMISSION AND SPACE CHARGE

To be emitted into vacuum, electrons that are in a metal cathode must overcome the potential barrier whose height is greater than the electron's Fermi energy. In the classical picture, the only way for the electron to escape is to get "over" the barrier by adding enough energy to the electron, as shown in Figure 30.

62
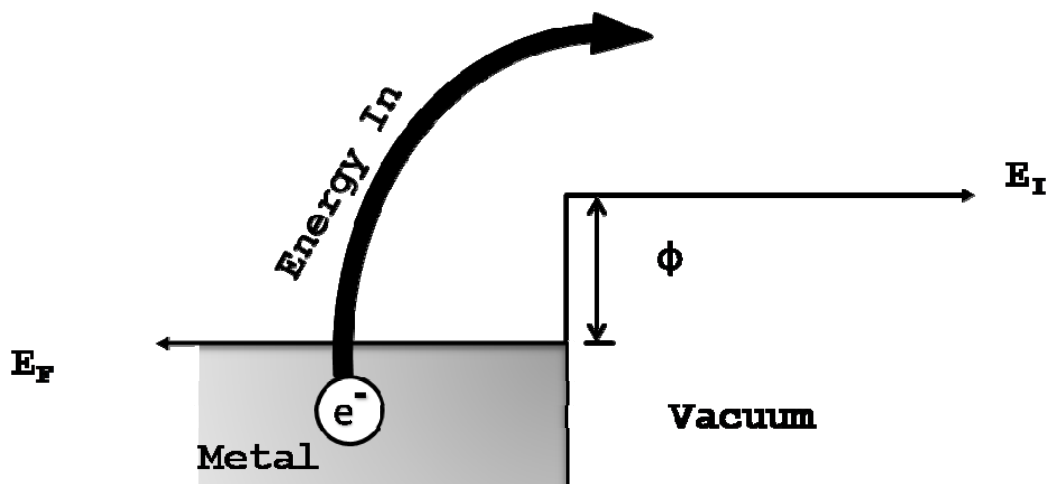
Figure 30. **Photoemission of an electron. An electron would increase in energy to rise from its Fermi energy to escape the metal. This is known as the work function of the material (φ). E$_F$ is the Fermi energy and E$_I$ is the ionization energy.**

But from quantum mechanics we know that there is some fraction of the particles that can be transmitted through the barrier by "tunneling". These electrons "tunnel" through the barrier instead of over it. To have an appreciable number of electrons transmitted through the barrier, we must make the barrier thickness small, which can be accomplished by applying a strong electric field to the cathode surface. The electric field, is determined by the potential gradient,

$$ E = -\frac{dV}{dx} \quad , \qquad (30) $$

where x is the distance away from the cathode surface and V is the potential at the cathode and E is the one-dimensional electric field. Once integrated, we see that if we can make the field very strong that we can increase the voltage at the surface and this affects the barrier. When the potential gradient is applied, the new barrier

shows a sloped profile that results from the high voltage applied a projected tunneling distance (dotted line), shown in Figure 31. By tunneling through the barrier, the electron would escape the surface of the metal into the vacuum. This process is known as "field emission."
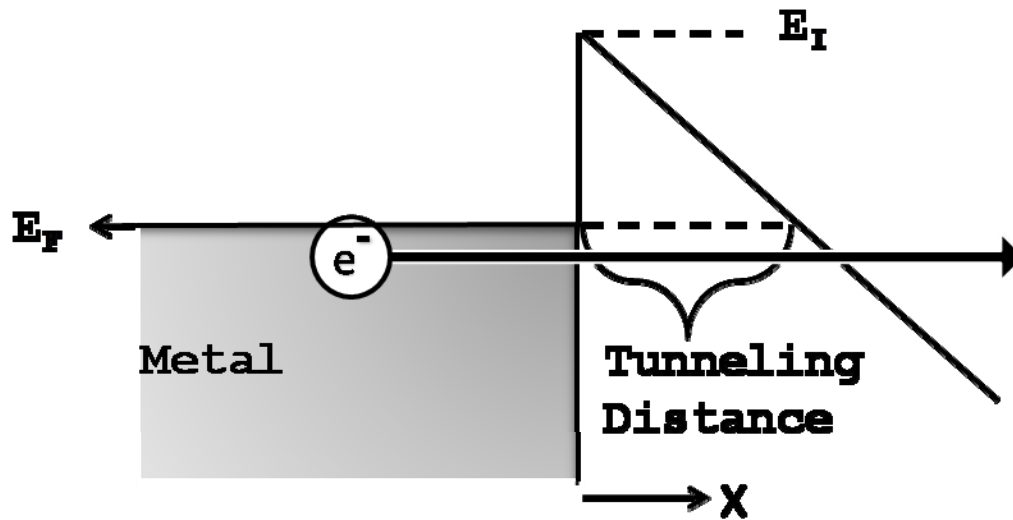
Figure 31. The barrier that the electron must tunnel through has been shortened due to the external electric field applied. This makes it possible for an appreciable number of electrons to tunnel through the barrier.

A higher field, *E,* reduces the thickness of the barrier and increases the probability of tunneling therefore increasing the extracted current. This dependence can be seen in the Fowler-Nordheim equation, which is the governing equation for field emission [8] and is

$$J \; = \; \frac{q^2}{2\pi h} \frac{1}{\phi + E_F} \sqrt{\frac{E_F}{\phi}} E^2 \; \exp- \left[\frac{8\pi}{3} \frac{\sqrt{2mq}}{h} \frac{\phi^{3/2}}{E} \right] \quad ,$$

$h \; = \; 6.6x10^{-34} \text{Joule} \times \text{seconds} \; ,$

$q \; = \; 1.6x10^{-19} \text{Coulomb} \; ,$

$E \; = \;$ applied electric field [volts/meter] ,

$m \; = \; 9.1x10^{-31} \text{kg} \; ,$

$\phi \; = \;$ Work Function [eV] ,

$E_F \; = \;$ Fermi Energy [eV] .

(31)

Introducing the functions *A* and *B* we can simplify the equation to a form that shows the dominant dependence of the electric field in the exponent,

$$J \; = \; AE^2 e^{-B/E} \quad ,$$

$$A \; = \; \frac{6.2x10^{-6}}{\phi + E_F} \left(\frac{E_F}{\phi} \right)^{1/2} \quad ,$$

$$B \; = \; 6.8x10^9 \phi^{1.5} \quad .$$

(32)

This gives a basis for predicts the emitted current density in a field emission process. The limitation however is that they are derived for a parallel plate and are not exact in real systems. However, they still provide a good description of the effects seen experimentally. [8]

The Child-Langmuir law gives the current limit due to space charge in a diode,

$$J \; = \; 2.33 \times 10^{-6} \frac{V_0^{3/2}}{d^2} \quad [\text{A/m}^2]$$

$V_0 \; = \;$ voltage difference [*volts*].

$d \; = \;$ seperation [*meters*]

(33)

Due to the space charge of the electrons, the potential at a given point lowers. Equation (33) gives the maximum steady-state current density that can occur between

two plates of a diode by just increasing the electron supply from the cathode. The only changes that can be made to increase the current density therefore are to increase the voltage difference or decrease the spacing between the anode and cathode.[9]

B.   MOTIVATION FOR A NEW EXPERIMENT: THE DIAMOND FIELD-EMITTER

For an FEL, the injector must be able to provide a bright electron beam with low emittance. This process must be reliable and have a long lifetime if it is to be feasible as a shipboard application. One of the hurdles to overcome is to provide high average current. NPS would like to gain experience with designs for possible use in the NPS FEL quarter-wave RF gun that will replace the Stanford DC injector.

Professors Charles Brau and Roy Davidson, at Vanderbilt University, are currently exploring the Diamond Field-Emitter Array (DFEA) shown in Figure 32. This is an electron microscope image of a DFEA from the top and then a side view of a single tip. The tips have small radii that provide the field enhancement necessary for field emission.
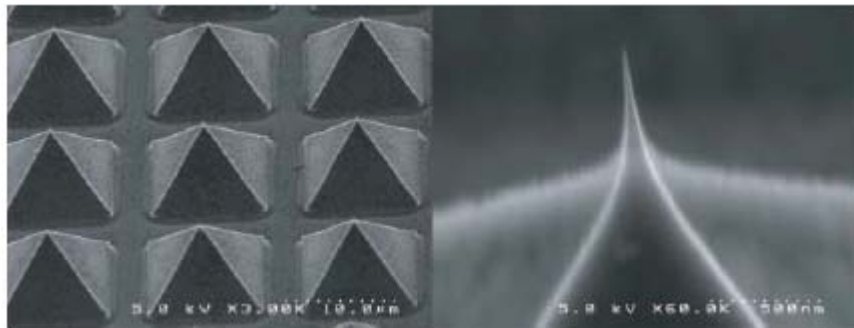

Figure 32.   Diamond Field-Emitter Array (DFEA) [From 10]

When strong voltages are applied to the tips of the array, gradients of the order of 10-20 MV/m result, and electrons will tunnel out of the tips of the diamond pyramids. Some of the advantages of these diamond field arrays are their durability, high thermal conductivity, and chemical inertness.

Unfortunately, the current DC gun at NPS does not have the flexibility to perform adequate characterization of DFEA cathodes. Since the cathode stalk is immovable, with the voltage fixed we cannot achieve more than 1.4 MV/m, which is not high enough to stimulate the emission from the DFEAs.

The test apparatus under use at Vanderbilt is shown in Figure 33. The test stand is experiencing vacuum arcing and physical damage from ion blowback off the gridded anode. The voltage source is small (only a few kV) and to reach the required field strength, an extremely small spacing between the anode and cathode is used (quartz capillary is the spacer). The electrons are bombarding the gridded anode causing ion blowback back to the diamond tips and substrate. This is damaging to the cathode and limiting the gradient that they can achieve, as well as their maximum currents and run times.
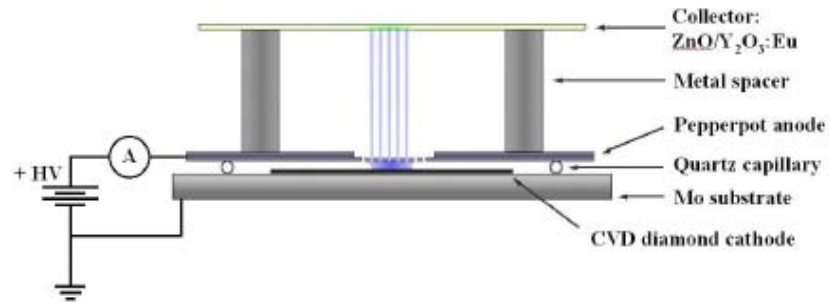
Figure 33.   Vanderbilt design for testing emittance.[From 11]

C.   DESIGN REQUIREMENTS FOR A NEW TEST CELL

To facilitate further research at NPS into the DFEA and other potential candidates, a new cathode test cell has been designed, shown in Figure 34.   It will be a static field emission design with fields that are adjustable at the cathode from approximately 5~20 MV/m.   The cathode will need to be capable of easy exchange to facilitate test and analysis of the cathode surface after bombardment, as well as to support rapid testing of different cathodes.
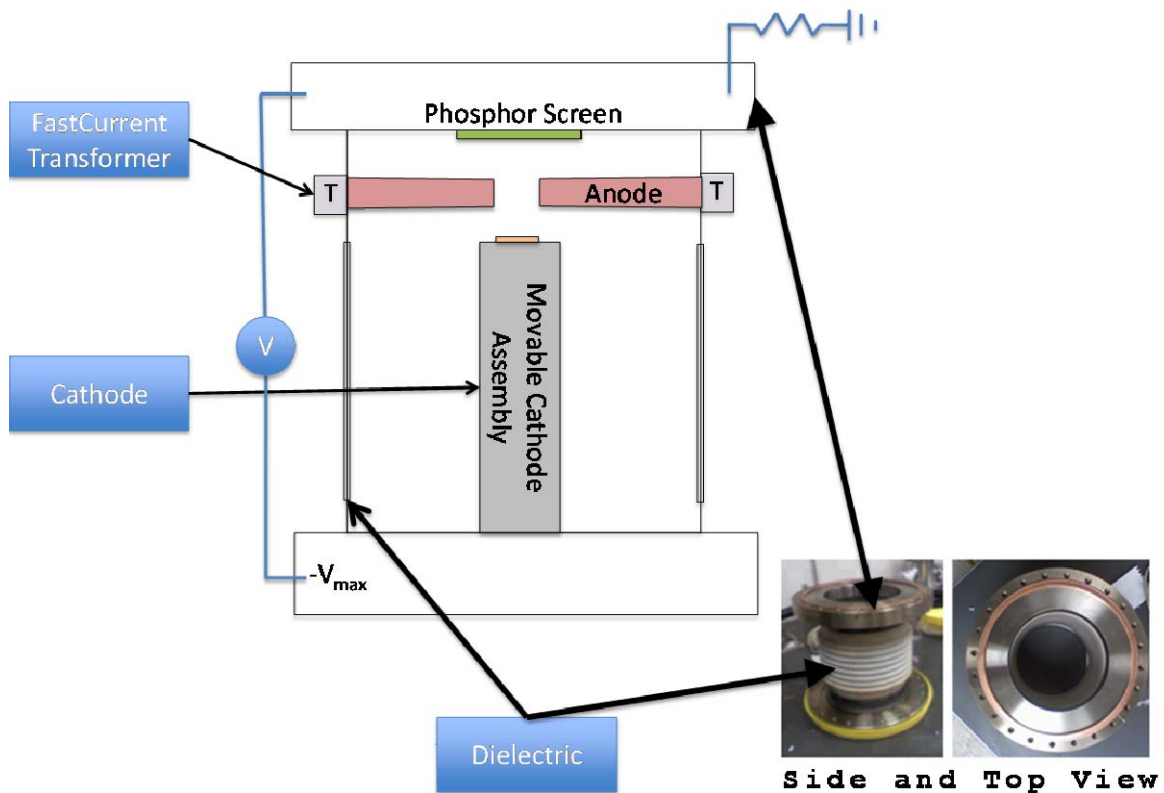
Figure 34.   **Basic Configuration of new Test Cell.**

The inspiration for the basic design was a vacuum chamber that NPS FEL group already possessed, shown in the bottom right of Figure 34. The top and bottom are metal flanges separated by a ceramic break. The flanges are a conflat type. Conflat is a standard design with many distributors that can sell parts that will bolt up directly. This allows easy connections for things such as the high voltage and diagnostic equipment.

We could vary the anode-cathode voltage by changing out the high voltage power supply. However, in our study we limited this to the 100 kV power supply already on hand. The spacing between the anode and cathode changes by (1)

manufacturing it to a fixed width or more preferably, (2) make the cathode stalk movable. The latter would allow studies with varying field strength at the tip of the DFEAs by simply moving the cathode stalk. As the spacing decreases, we will be able to see the field at the tips of the DFEA increase. The trade off is that the conditions for vacuum arcing also increase with the increasing field strength.

Some of the diagnostics will include a phosphor screen at the end of the cell and beam current measurement devices. The phosphor screen will allow for preliminary beam shape characterization with proper spacing of the tips in the DFEA. By measuring the voltage across a resistor attached to the anode, we can measure the current being produced by the DFEA. The current transformer would allow for measurements of the stability of the electron beam current, as any fluctuation in the beam current would show up as a voltage fluctuation on the coil.

The proposed test cell design will allow for a separation between the phosphor screen and the cathode. By placing the anode and the phosphor screen at the same potential and putting a chamber between the two, a minimal amount of blowback from ions will be experienced compared to the Vanderbilt design. We may be able to achieve higher field than Vanderbilt due to decreased ion damage anticipated. However, we will have to live with some amount of defocusing that would not occur with the closely spaced gridded cathode. This is because in the gridded cathode, the field lines are uniform across the small gap (equivalent to a parallel plate capacitor).

70

D.   GEOMETRIES CONSIDERED

The three significant issues motivating geometry choices are (1) uniform field activation, (2) preventing vacuum arcing, and (3) achieving sufficient fields at the cathode to extract an appreciable current. Multiple configurations are evaluated using the software developed at Lawrence Livermore National Laboratory, *Superfish.* The software runs on a desktop and is publically available for download from the laboratories website [ref]. It provides electrostatic data of the test cell, such as electric field values and equipotential lines, and is used in this study to compare two basic geometries.

An example that gives a sample output for the two basic geometries studied is in Figure 35. The top left geometry has an anode with the top portion angled away from the intended trajectory of the electron beam. In the bottom-left geometry, the top angle is removed and the bottom portion of the anode is angled away from the cathode stalk. Note that this picture, which is representative of *Superfish's* output, is only half of the cross-section of the area of interest, using radial symmetry. In following figures, the output has been modified in order to better give the reader a physical picture of the cavity characteristics.

An angle on the upper portion of the anode is beneficial. As the electrons travel through the cavity to the phosphor screen, they will spread due to space-charge effects and defocus. If the anode angles away from the surface of the cathode, the potential for vacuum arcing may be reduced.

Along with the basic shape changes, the gap between the anode and cathode was varied. The spacings used were 1 cm, 0.5 cm, and 0.25 cm gap for both geometries. Two apertures, 0.5 cm and 0.25 cm, were looked at for the widest anode-cathode gap of 1 cm.
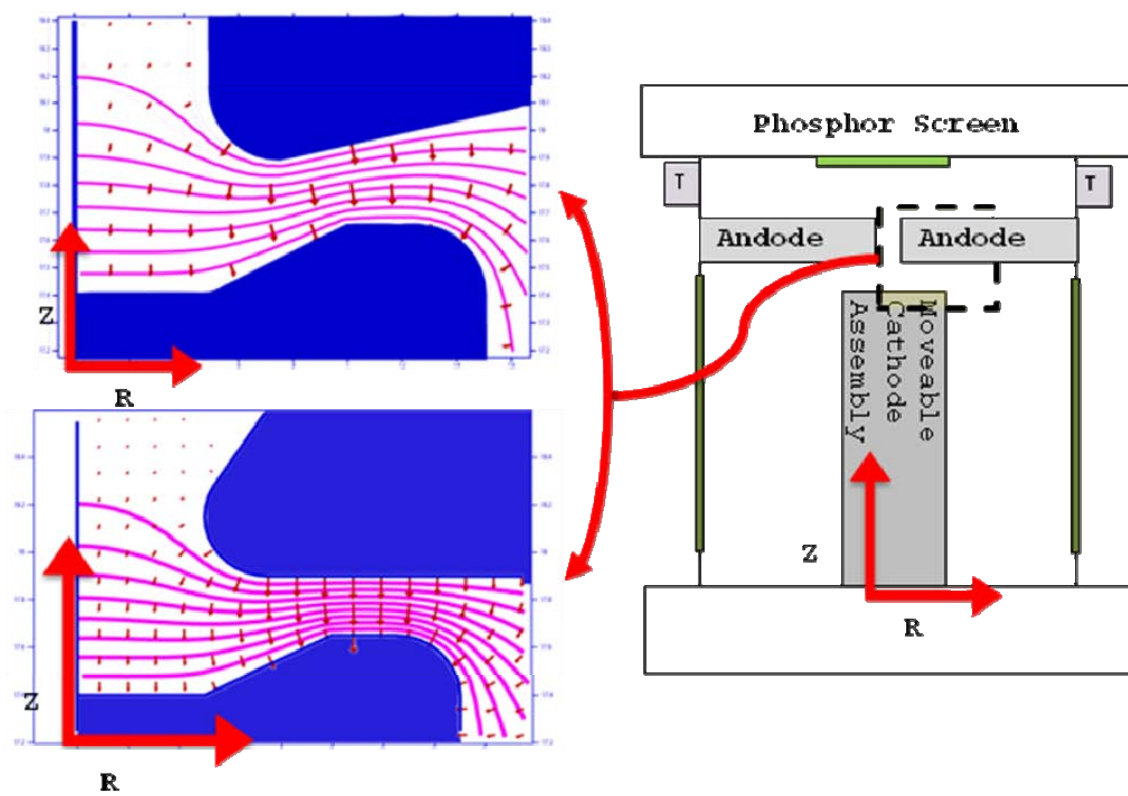
Figure 35.   Proposed cathode test cell and two
geometries studied using Superfish.

E.   RESULTS

The field strength along the cathode surface for all configurations is presented in Figure 36.   Recall that a target range of 6–15 MV/m field is desired for the cathode. The varying shapes of the anode made little difference to the maximum field at the center of the cathode, or the uniformity it was across the surface.   The field strength was a function of the anode to cathode gap as predicted by equation (30).   The target range for field strength is achieved and the results for the 0.5 cm anode aperture and the various anode cathode gaps are given in Table 4.

The uniformity of the field across the cathode was also dependent on the anode to cathode gap.   For the smallest gaps the field strength varied less than 1% up to 0.3 cm from the center.   The largest gap of 1 cm was similarly uniform out to only 0.13 cm. The change in anode shape and aperture did not appreciably affect the uniformity.

The maximum field strength in each case was not dependent on anode aperture, but was a function of both the anode-to-cathode gap and the anode shape. A maximum of 49 MV/m was found for the top angled anode with a spacing of 0.25 cm. The bottom angled anode with same spacing resulted in a lower 40 MV/m. As the anode to cathode gap was increased, the maximum field decreased to 20 and 18 MV/m showing that as the gap was increased the anode shape had less influence.
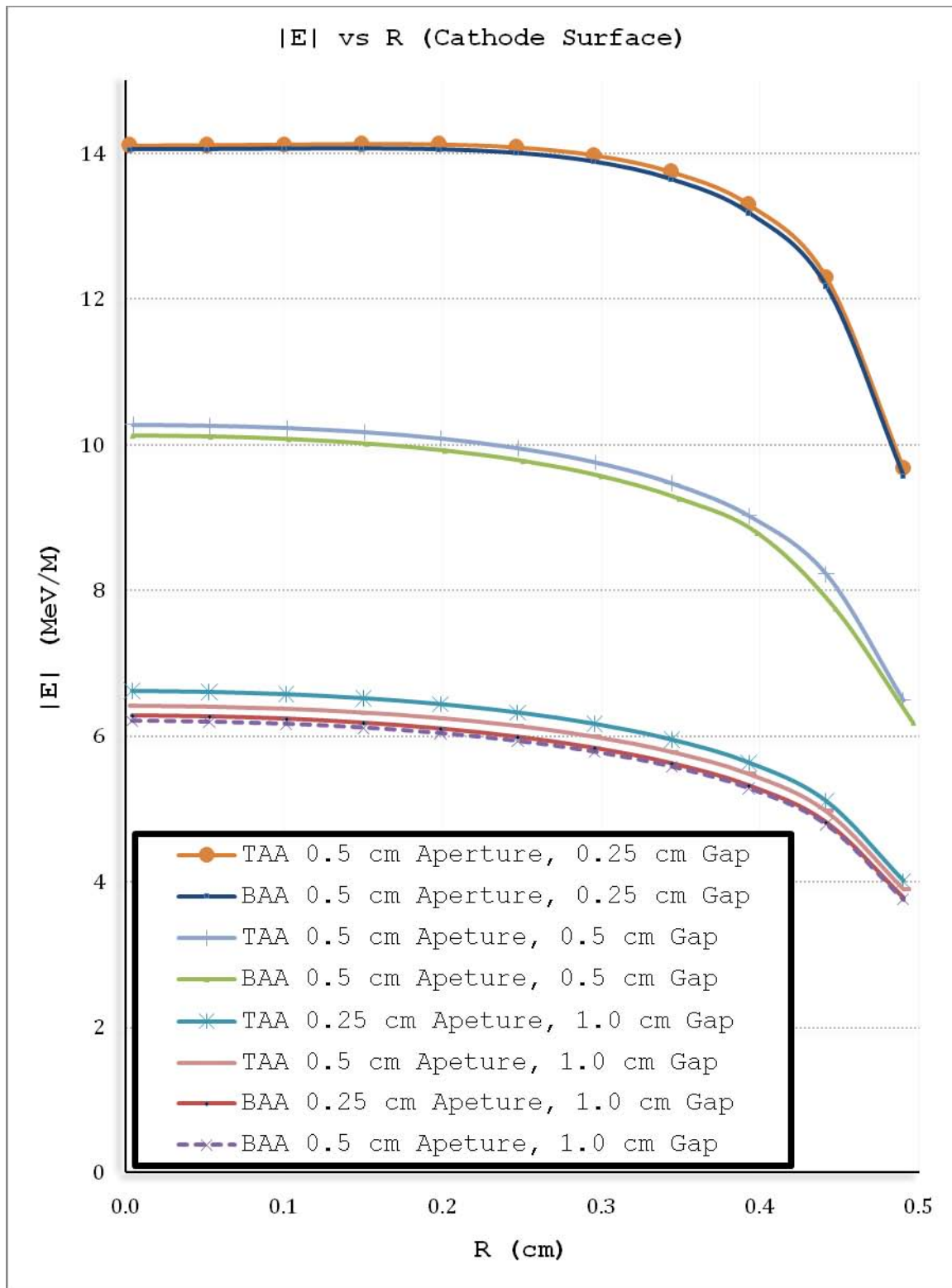
74

Figure 36. Field strength at Cathode versus radius for Bottom Angled Anode (BAA) and Top Angled Anode (TAA).

When varying the gap in the top angled anode the defocusing at the anode increases as the spacing decreases, shown in Figure 37. The electron beam in the smaller gap experiences a higher field near the cathode and would be accelerated over a shorter distance. This would allow the beam to reach higher velocities before it diverges appreciably. This will aid in the increased defocusing that will occur once it reaches the anode for the smaller gap configuration. Unfortunately, when the gap is smaller, the focusing immediately after leave the cathode is decreased since the field lines appear flatter in Figure 37.

When compared to the bottom-angled anode, it is evident that the maximum field is higher for the top angled anode, as shown in Figure 38. The figure shows that when the anode bottom is angled away from the cathode stalk, the equipotential lines are allowed to spread out and decrease the magnitude of the field. Both geometries appear to have similar defocusing characteristics for the electron beam as it exits the anode aperture.

When the aperture is decreased, the defocusing at the aperture is reduced, as shown in Figure 39. The rest of the cavity is not significantly affected by the change.

Figure 37.   Equipotential and electric field map for Top
Angled Anode: various gaps. The gap is decreased from top
to bottom, 1 cm, 0.5 cm and 0.25 cm, respectively.
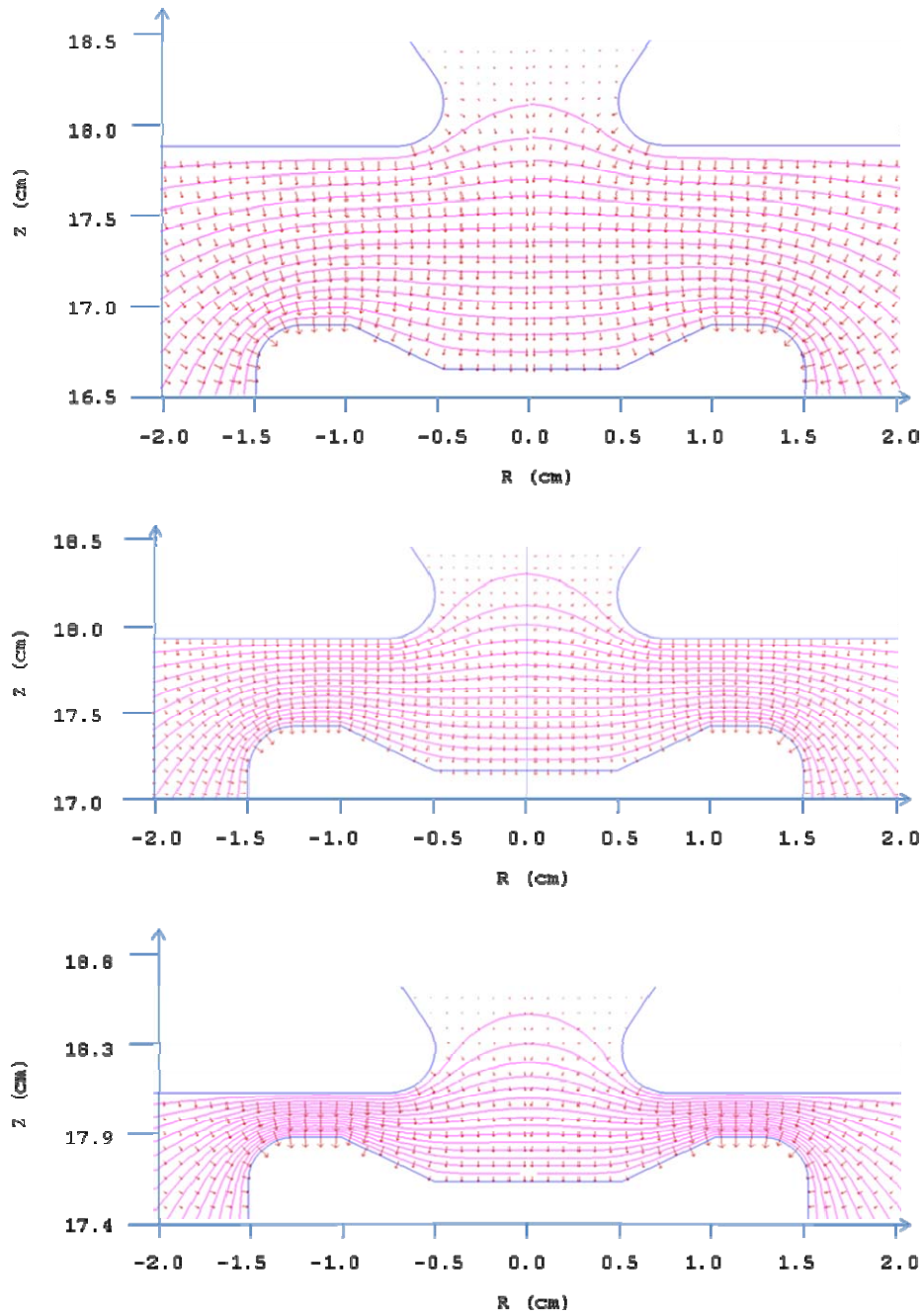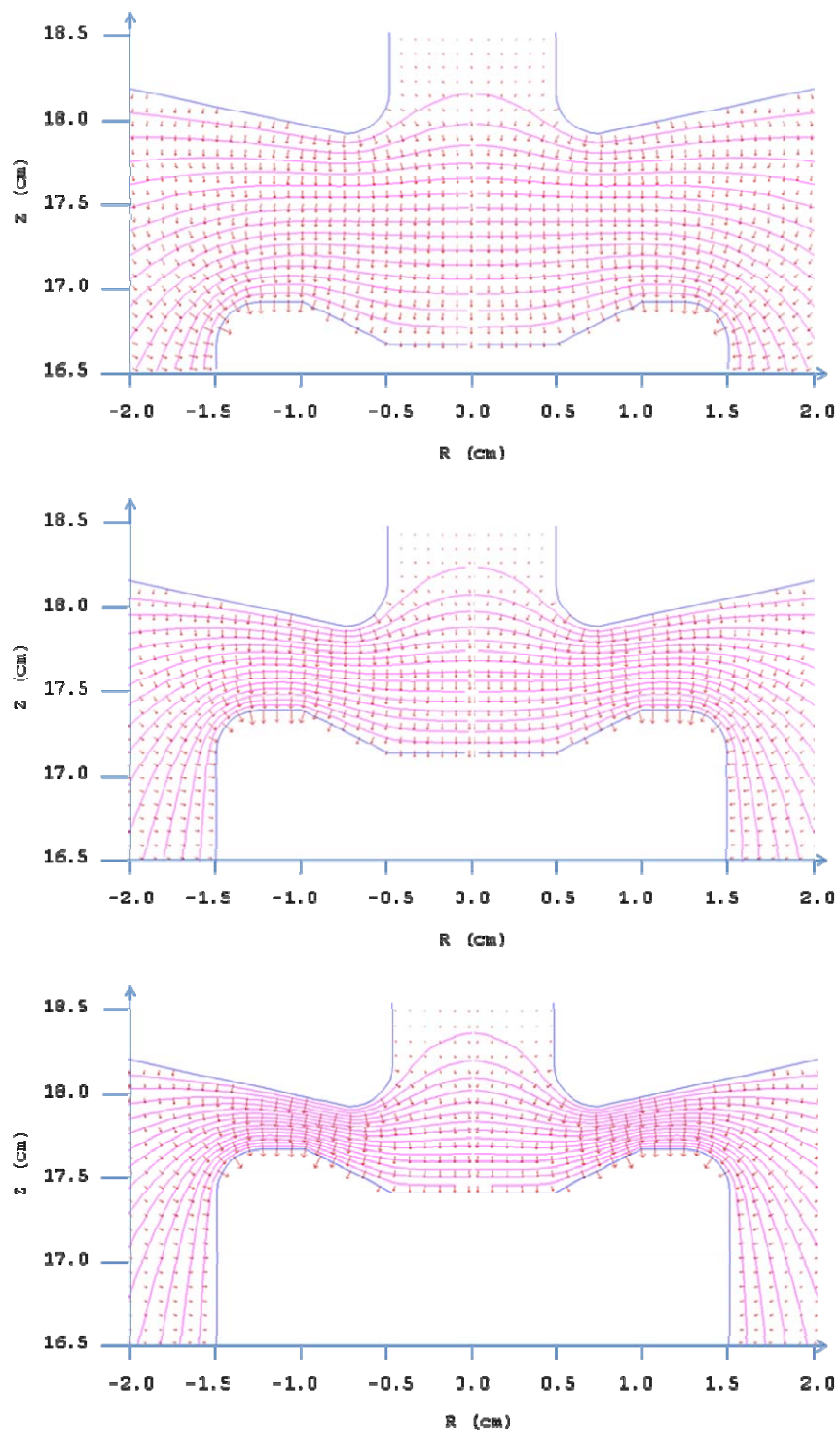
Figure 38.   Equipotential and electric field map for
bottom angled anode: various gaps.   The gap is decreased
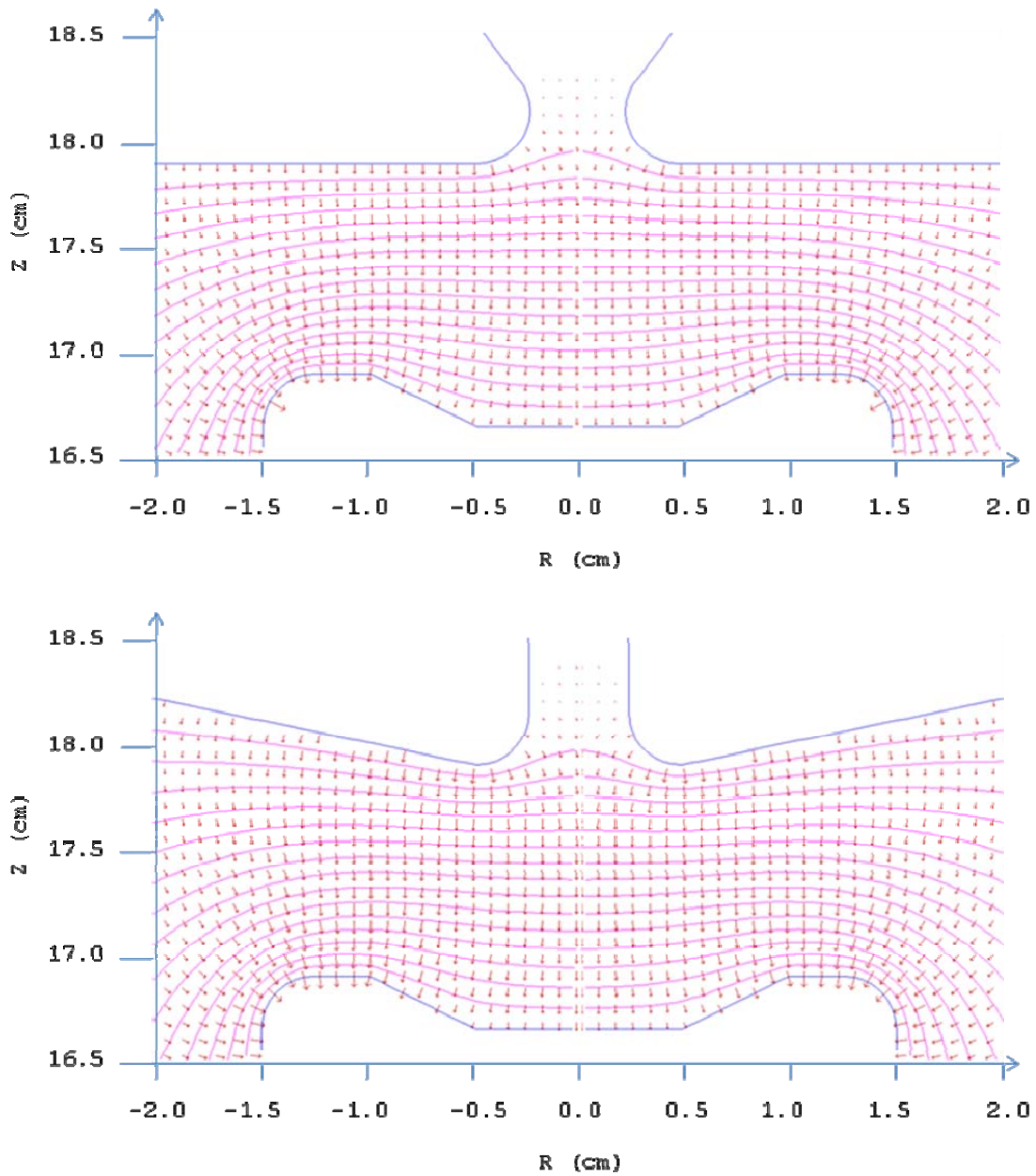from top to bottom; 1 cm, 0.5 cm and 0.25 cm, respectively.

Figure 39. Equipotential and field map for top angled anode (top) and bottom angled anode (bottom) with a smaller aperture of 0.25 cm.

F. RECOMMENDATIONS

The geometries presented meet the criteria for providing an electric field strong enough for activation of the DFEA, and uniform enough to be able to begin to characterize the array's performance. If fields at the upper end of the range are to be utilized careful consideration to the cathode manufacturing, or altering the design, will be needed to ensure that vacuum arcing is not an issue. The bottom-angled anode would be the easiest to modify to ensure this is not an issue. Decreasing the anode aperture returns little payoff when compared to the risk of clipping the electron beam and is not recommended. A summary of the key results is presented in Table 4. Only the 0.5 cm aperture is included and the maximum electric field in the cavity, maximum field on the cathode and radius of cathode that experiences less than a 1% change in field strength are included.

The two geometries both have their advantages. The process to prevent breakdown in a high voltage system like this is much more difficult then installing more diagnostic equipment that can monitor and account for electron bombardment onto the anode surface. For these two reasons and based on the result presented the bottom anode design is recommended for design completion and fabrication.

Bottom Angled Anode (BAA)	Max Field (MeV/M)	Max Cathode Field (MeV/M)	1% Cathode Field Change (cm)
0.25 cm	40	14	0.3
0.5 cm	25	10	0.15
1.0 cm	18	6.2	0.12

Top Angled Anode (TAA)	Max Field (MV/M)	Max Cathode Field (MV/M)	1% Cathode Field Change (cm)
0.25 cm	49	14	0.3
0.5 cm	29	10.2	0.15
1.0 cm	20	6.4	0.13

Table 4.   Summary of 0.5 cm aperture geometries.

THIS PAGE INTENTIONALLY LEFT BLANK\

LIST OF REFERENCES

[1] G. Roughead, Admiral, U.S. Navy. "Memorandum for Director, Strategic Studies Group." 21 September 2009.

[2] William B. Colson, Class Notes, "PH 4911-Simulation of Physical and Weapon Systems." Winter 2009.

[3] "Free Electron Laser." Wikipedia, the free encyclopedia, http://en.wikipedia.org/wiki/Free_electron_laser (October 2009).

[4] Joseph Blau, Dissertation- "Multimode Simulations of Free Electron Lasers" March 2002.

[5] Tomas Jefferson National Accelerator Facility. FEL description http://www.jlab.org/FEL/feldescrip.html (October 2009).

[6] P. B. Crooker, W. B. Colson, J. Blau, J. Aguilar. "Short Rayleigh Length Free Electron Laser: Experiments and Simulation." Physical Review Special Topics: Accelerators and Beams (2008).

[7] J. W. Lewellen, "The NPS-FEL Injector Upgrade." Proceedings of LINAC08, Victoria, BC, Canada (2008).

[8] S.T. Pai & Qi Zhang, "Introduction to High Power Pulse Technology." World Scientific (1995).

[9] M. Reiser. "Theory and Design of Charged Particle Beams." Wiley (1994).

[10] C.L. Stewart, "Thesis: Measurement of Energy Spectrum of Electrons Field-Emitted from Diamond Field-Emitter Arrays." Vanderbilt University (2009).

[11] J.D. Jarvis, & Andrews, H. L. & Brau, C. A., "Transverse Emittance of Diamond Field-Emitter Arrays." Proceedings of FEL08, Gyeongju, Korea (2008).

THIS PAGE INTENTIONALLY LEFT BLANK

INITIAL DISTRIBUTION LIST

1. Defense Technical Information Center
    Ft. Belvoir, Virginia

2. Dudley Knox Library
    Naval Postgraduate School
    Monterey, California

3. Chairman, Department of Physics
    Naval Postgraduate School
    Monterey, California

4. Prof. William B. Colson
    Naval Postgraduate School
    Monterey, California

5. Quentin Saulter
    Office of Naval Research
    Arlington, Virginia

6. Michael Deitchman
    Office of Naval Research
    Arlington, Virginia